Bioorganic Chemistry 87 (2019) 395–408

Contents lists available at ScienceDirect

Bioorganic Chemistry

journal homepage: www.elsevier.com/locate/bioorg

Design, synthesis and evaluation of chalcone Mannich base derivatives as multifunctional agents for the potential treatment of Alzheimer's disease

Xiaoyu Zhang, Qing Song, Zhongcheng Cao, Yan Li, Chaoquan Tian, Ziyi Yang, Heng Zhang, Yong Deng*

Department of Medicinal Chemistry, Key Laboratory of Drug-Targeting and Drug Delivery System of the Education Ministry, Sichuan Engineering Laboratory for Plant-Sourced Drug and Sichuan Research Center for Drug Precision Industrial Technology, West China School of Pharmacy, Sichuan University, Chengdu 610041, PR China

ARTICLE INFO

Keywords:
Alzheimer's disease
Chalcone Mannich base derivatives
Acetylcholinesterase inhibitors
MAO-B inhibitors
Antioxidant
Aβ aggregation inhibitors
Multifunctional agents

ABSTRACT

A series of chalcone Mannich base derivatives were designed, synthesized and evaluated as multifunctional agents for the treatment of Alzheimer's disease based on the multi-target directed ligands design strategy. *In vitro* assays demonstrated that most of the derivatives exerted potent selective inhibitory potency on AChE with good multifunctional properties. Among them, representative compound **7c** exhibited moderate inhibitory potency for *Ee*AChE (IC_{50} = 0.44 μM) and MAO-B inhibition (IC_{50} = 1.21 μM), good inhibitory effect on self-induced $A\beta_{1-42}$ aggregation (55.0%, at 25 μM), biometal chelating property, moderate antioxidant activity with a value 1.93-fold of Trolox. Moreover, both kinetic analysis of AChE inhibition and molecular modeling study revealed that **7c** showed a mixed-type inhibition, binding simultaneously to CAS and PAS of AChE. In addition, **7c** also displayed high BBB permeability. These properties indicated **7c** may be a promising multifunctional agent for the treatment of AD.

1. Introduction

Alzheimer's disease (AD), the most major cause of dementia in the elderly, is a chronic and age-associated neurodegenerative disorder characterized by progressive and irreversible cognitive deterioration, behavioral disturbances and memory loss. With the increase of average life expectancy, AD has become severe familiar, social, and economic problem. Although extensive efforts have been made to understand the complex pathophysiology of AD, its exact etiology is still unknown [1]. There are several hallmarks, such as low levels of acetylcholine (ACh), the formation of β-amyloid (Aβ) deposits, τ-protein hyperphosphorylation, oxidative stress and biometals dyshomeostasis, have been considered to play significant role in AD pathogenesis [2,3].

The deficit of ACh in specific brain regions is a central event in the pathogenesis of AD according to the cholinergic hypothesis, as it is demonstrated to be able to induce pathogenic cascade, ultimately leading to cognitive impairment and dementia [4]. Acetylcholinesterase (AChE) and butyrylcholinesterase (BuChE) are the main enzymes responsible for the hydrolysis of neurotransmitter ACh [5]. Increasing sentiment that AChE plays a dominant role in the degradation of ACh, which is closely associated with the pathology of AD [6]. Moreover, BuChE has been found to functions as an auxiliary enzyme and serves as a co-regulator in regulating the ACh level. However, serious inhibition of BuChE may contribute to the peripheral side effects of cholinesterase inhibitors mainly associated with their peripheral ChE inhibitory activity [7]. Taking these reasons into consideration, it may be an effective therapeutic strategy to develop novel selective AChE inhibitors as the treatment of AD [8].

Monoamine oxidases (MAOs) are flavin adenine dinucleotide (FAD) containing enzymes that catalyze the deamination of a variety of biogenic and xenobiotic amines [9]. There are two distinct enzymatic isoforms of MAOs, including MAO-A and MAO-B. Selective inhibitors of MAO-A have been demonstrated to have therapeutic utility for the treatment of depression while MAO-B inhibitors are used in several neurodegenerative disorders such as Parkinson's disease (PD) and Alzheimer's disorder [10]. Selegiline, a selective MAO-B inhibitor, was found to improve learning and memory deficits associated with AD in animal models [11]. More study showed high expression levels of MAO-B in neuronal tissue could result in an increase in the level of oxidative free radicals, which play a major role in the aetiology of AD [12]. Therefore, selective MAO-B inhibitors were considered to be potential candidates for anti-Alzheimer disease drugs.

Besides, numerous research groups suggested that oxidative stress and abnormal metabolic oxidative reactions in the central nervous

* Corresponding author.
E-mail address: dengyong@scu.edu.cn (Y. Deng).

https://doi.org/10.1016/j.bioorg.2019.03.043
Received 29 December 2018; Received in revised form 22 February 2019; Accepted 15 March 2019
Available online 19 March 2019

system (CNS) may play important role in the pathogenesis of AD [13]. Reactive oxygen species (ROS), which formed during normal metabolic reactions, is kept relatively low levels by efficient antioxidant system. However, the excess generation of ROS may disequilibrate the balance of endogenous antioxidant systems and result in oxidative stress [14]. Interestingly, the dyshomeostasis of biometals, especially the abnormal accumulation of redox-active metal ions, is involved in the production of ROS and subsequent oxidative stress [15]. Inspired by these illustrations, modulation of special biometals in the brain or the development of anti-oxidants, is currently a potential therapeutic strategy to anti-AD.

According to the amyloid hypothesis, the intracellular neurofibrillary tangles (NFTs) and extracellular deposition of Aβ peptides also play pivotal role in the pathogenesis of AD, which trigger a cascade of biochemical events, such as the formation of senile plaques, neuronal cell loss, and cerebral atrophy [16]. The $A\beta_{1-40}$ and $A\beta_{1-42}$ are the main isoforms of Aβ, and $A\beta_{1-42}$ exhibits higher cytotoxicity than $A\beta_{1-40}$ [17]. Furthermore, some studies indicated that the abnormal accumulation of metals ions, such as Cu^{2+}, Fe^{2+}, Zn^{2+} and Al^{3+}, may induce the formation of Aβ plaques and NFTs [18]. Consequently, the prevention of $A\beta_{1-42}$ aggregation seemed to be a rational approach for AD treatment.

Given the complexity of AD, the current available single target drugs including cholinesterase inhibitors and *N*-methyl-*D*-aspartate (NMDA) receptor antagonist mainly focused on the symptomatic aspects and could not prevent progressive neurodegeneration effectively. Thus, the development of agents that affect two or more biological activities associated with AD has drawn considerable attention for their advancement in the treatment of AD [19–22]. Chalcones (Fig. 1, **I**), *trans* 1,3-diphenyl-2-propen-1-ones, are considered to be precursors of flavonoids and isoflavonoids [23]. Studies showed that chalcones possess a wide spectrum of pharmacological properties, such as antioxidant, anti-inflammatory and neuroprotective effect [24–26]. Recently, many studies also demonstrated that natural chalcone and synthetic analogs exhibited ChE and MAO inhibitory activities, and were more commonly used as Aβ imaging agents [27–29]. Therefore, the development of chalcone derivatives endowed with several advantages may become an active field in the current AD research. Recently, some researches showed that molecules bearing phenolic Mannich base moieties (Fig. 1, **II**) may exhibit good antioxidant [30], AChE inhibitory activity [31] and biometal chelating properties [32]. Mannich base have received the increasing consideration due to physiologically reactivity of the basic function rendering the molecule soluble in aqueous solvents when it is transformed into ammonium salt [33]. Herein, based on the multitarget-directed ligands (MTDLs) strategy, chalcone scaffold was selected to combine with different amino group to design a series of chalcone Mannich base derivatives, in the hope of acquiring these novel molecules possessing more potency in the therapy of AD.

In this study, a series of novel chalcone Mannich base derivatives were designed (Fig. 1), synthesized and evaluated for their biological activity, including the inhibition of cholinesterase and MAOs activity, the inhibition of Aβ aggregation, antioxidant properties, biometal chelating effects and the ability to cross the blood–brain barrier (BBB).

2. Results and discussion

2.1. Chemistry

The synthetic pathways of target derivatives were summarized in Schemes 1–5. Synthesis of 3′-OH chalcone Mannich bases **7–10** are shown in Scheme 1. The 3′-OH chalcones **4–6** were the key intermediates, derived *via* the condensation of substituted acetophenones with *m*-hydroxy benzaldehyde in the presence of 50% KOH and EtOH [34–37]. Then the corresponding target compounds **7–9** were afforded by the Mannich reaction of key intermediates **4–6** with various

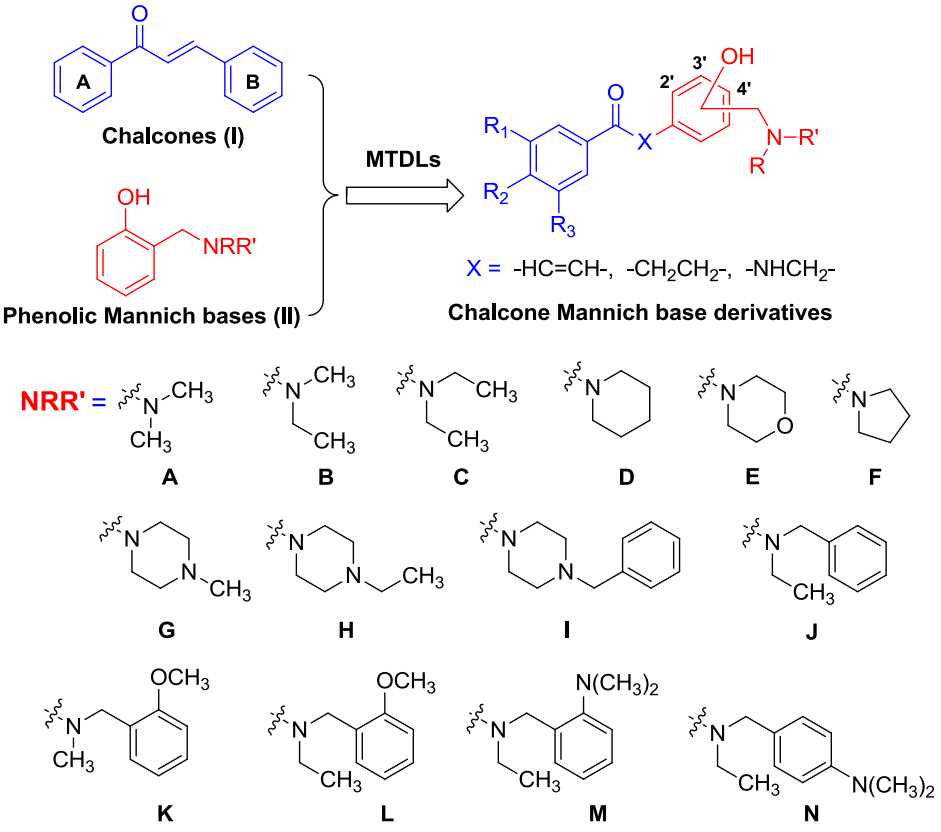

Fig. 1. Design strategy for the chalcone Mannich base derivatives.

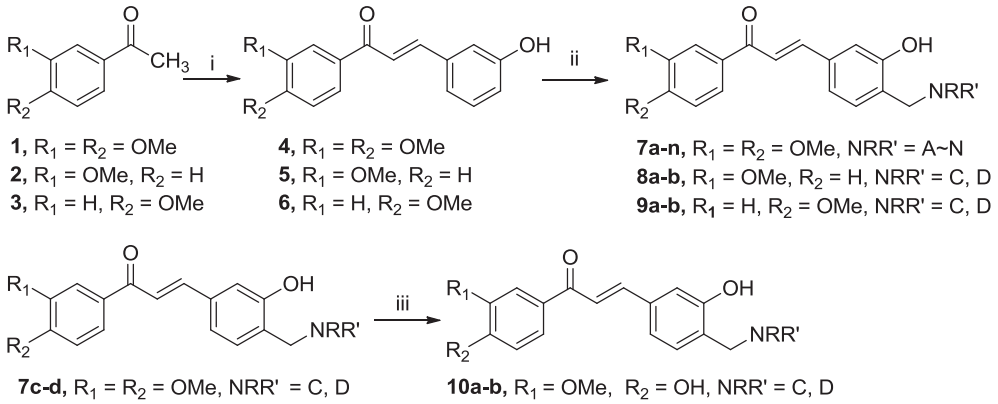

Scheme 1. Synthesis of 3′–OH chalcone Mannich base **7**–**10**. *Reagents and conditions:* (i) *m*- hydroxybenzaldehyde, 50% KOH, EtOH, r.t., 4–24 h; (ii) paraformaldehyde, secondary amine (HNRR′), EtOH, reflux for 24–48 h; (iii) $AlCl_3$, CH_2Cl_2, r.t., 6 h.

secondary amines (HNRR′) and paraformaldehyde in EtOH [33,38]. The formation of *o*-substituted products in the Mannich reaction is attributed to the hydrogen bonding between nitrogen and the *o*-hydroxy group, which form a stable six-membered ring [38]. 4-OH chalcone derivatives **10a-b** were prepared from **7c-d** by demethylation with $AlCl_3$ in CH_2Cl_2. The *para*-demethylated product might be facilitated by the electron withdrawing nature of carbonyl group and $AlCl_3/CH_2Cl_2$ acts as an efficient regioselective demethylating agent [39].

For the synthesis of 3′-OH dihydrochalcone Mannich base **11**, compound **7d** was hydrogenated in the presence of 10% Pd/C to obtain **11** in good yield [40], as shown in Scheme 2.

Synthesis of 3′-OH chalcone bis-Mannich bases **13a-b** are shown in Scheme 3. Treatment of **4** in $AlCl_3/CH_2Cl_2$ system gave intermediate **12** [39], which subsequently reacted with different secondary amines and paraformaldehyde in EtOH to give the corresponding target compounds **13a-d** [33,38].

The chalcone scaffold (**14**) was the key intermediate for the synthesis of 4′-OH chalcone Mannich bases **15a-b** (Scheme 4), which derived *via* the condensation of substituted acetophenones with *p*-hydroxybenzaldehyde in the presence of 50% KOH and EtOH [34–37]. Then the corresponding target compounds **15a-b** were afforded by the Mannich reaction of key intermediate **14** with various secondary amines and paraformaldehyde in EtOH [33,38].

The general procedure for the synthesis of benzoyl benzylamine Mannich bases **22–24** are depicted in Scheme 5. Compounds **19–21** were the key intermediates, derived *via* the condensation of benzoic acid **16–18** and 3-(aminomethyl)phenol in the presence of 1-Ethyl-3-(3-dimethylaminopropyl) carbodiimide hydrochloride (EDCI) and 1*H*-benzo[d] [1,2,3]triazol-1-ol (HOBt) in THF [41]. Mannich reactions of **19–21** with paraformaldehyde and dimethylamine hydrochloride in EtOH gave the target compounds **22–24** [33,38].

All target compounds were characterized by ^{1}H NMR, ESI-MS and most of them were further characterized by ^{13}C NMR. The chemical structures of chalcone Mannich base derivatives are depicted in Table 1.

2.2. Pharmacology

2.2.1. Evaluation of AChE and BuChE inhibitory activities

The inhibitory activities of target compounds towards AChE (from *electric eel*) and BuChE (from rat serum) were evaluated, using Ellman's method with donepezil as the reference standard [42]. Inhibitory activities were summarized in Table 2. It indicated that these derivatives exhibited good *Ee*AChE inhibitory activities and scarcely any BuChE inhibitory activities. Among the tested derivatives, **13a** was the most potent for AChE inhibitory activity (IC_{50} = 0.07 μM). Structure-activity relationship analysis showed that the AChE inhibitory potency was closely related to the amine moiety and its substituted position, and the number of -OMe also have some impact. Generally, the aliphatic amine substituted compounds possessed greater AChE inhibitory activities than the benzylamine substituted compounds. Interestingly, **7e** expressed about 3–20 fold lower activity than derivatives **7a-d** and **7f**, which suggested that the electron-withdrawing effects of oxygen atoms at morpholine unit might reduce the electronic density of amines and further impact on its protonation, and finally affecting the interaction between the terminal nitrogen and *Ee*AChE. And the inhibitory results of **7c**, **7d**, **15a** and **15b** (IC_{50} = 0.44 μM, 0.49 μM, 38.7 μM, 24.3 μM, respectively) demonstrated that compounds with amines substituted at 4′-position were more appropriate for the AChE inhibitory potency than those at 3′-position. Moreover, compared with **7c** and **7d**, the bis-Mannich bases **13a** (IC_{50} = 0.07 μM) and **13b** (IC_{50} = 0.18 μM) were more appropriate for the AChE inhibitory potency. Compounds **22–24** and **11** displayed decreased trend of the inhibitory potency compared to compounds **7a** and **7d**, respectively, indicating changes of propylene ketone structure in chalcone such as the introduction of amide bond or reduction of alkene might have adverse impact to their activities against AChE.

2.2.2. Kinetic studies of AChE inhibition

To further study the mechanism of action of these derivatives on AChE, **7c** was selected for kinetic analysis using *Ee*AChE. The graphical presentation of the inhibition data of **7c** is shown in Fig. 2. The reciprocal Lineweaver-Burk plots showed that both slopes and intercepts were increased at increasing concentration of the inhibitor, which indicating that **7c** might behave as a mixed-type inhibitory in the presence of AChE. Replots of the slope versus concentration of **7c** gave an estimate of the inhibition constant (K_i = 0.23 μM).

2.2.3. Molecular docking studies of AChE

To further investigate the binding mode of the inhibitors with AChE, molecular modeling study was carried out with the representative

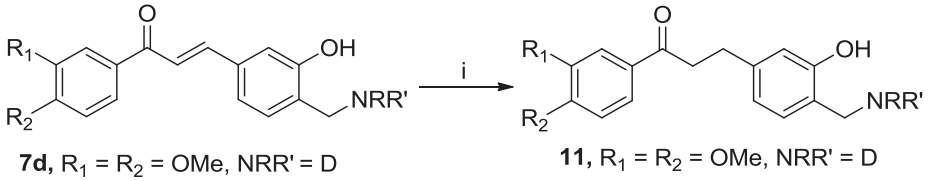

Scheme 2. Synthesis of 3′–OH dihydrochalcone Mannich base **11**. *Reagents and conditions:* (i) 10% Pd/C, H_2, THF, r.t., 10 h.

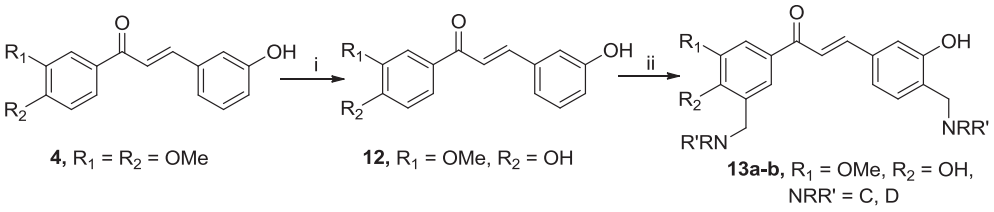

Scheme 3. Synthesis of 3′–OH chalcone bis-Mannich base **13a-b**. *Reagents and conditions:* (i) $AlCl_3$, CH_2Cl_2, r.t., 6 h; (ii) paraformaldehyde, secondary amine (HNRR′), EtOH, reflux for 48 h.

compound **7c** using the docking program, AutoDock 4.2 package [7]. Considering the high degree of homology between *Ee*AChE and *Tc*AChE, the X-ray crystal structure of *Tc*AChE (PDB code: *1EVE*) was chosen for our molecular modeling investigation. As shown in Fig. 3, compound **7c** could perfectly fit into the gorge of AChE and simultaneously interact with both the catalytic and peripheral site of AChE. In the *Tc*AChE-**7c** complex, the terminal *N*-benzyldiethylamine moiety could establish a hydrophobic interaction with Tyr121. The phenyl ring substituted with methoxy groups was observed to bind to the PAS of AChE and exhibited a potential hydrophobic interaction with residues Phe288 and Tyr334. In addition, a strong hydrogen bond was observed between the 3′-hydroxyl group and Asp72. Besides, the skeleton of chalcone folded in a conformation in the gorge that allowed them to interact with Phe288, Phe331 and Tyr334 *via* the hydrophobic interaction. The docking study showed that **7c** was a mixed-type inhibitor of AChE, which was consistent with our kinetic analysis result.

2.2.4. Antioxidant activity

The antioxidant activity of the derivatives was evaluated by the oxygen radical absorbance capacity assay that uses fluorescein (ORAC-FL) [43]. The results were displayed as Trolox (a water-soluble vitamin E analogue, which was used as a standard) equivalent. As shown in Table 2, all of the compounds showed moderate to good peroxyl radical absorbance capacities with ORAC-FL values ranging from 0.82 to 2.21 Trolox equivalents. In particular, **7b** and **24** exerted the most potent antioxidant activity with ORAC-FL values of 2.21 and 2.15 Trolox equivalents, respectively. And the representative compound **7c** also displayed significant antioxidant activity with a value 1.93-fold of Trolox. Meanwhile, **22–24** showed a rising trend of antioxidant activity with ORAC-FL values of 1.88, 2.04 and 2.15 Trolox equivalents, respectively. It indicated that the quantity of methoxy group may have some influence on the radical scavenging ability. In general, the aliphatic amine substituted compounds possessed higher antioxidant activities than the benzylamine substituted compounds. However, the substituted positions of the hydroxyl group and the amines showed no significant influence on the potency.

2.2.5. Studies of metal-chelating properties

The chelating ability of compound **7c** toward biometals such as Cu^{2+}, Fe^{2+}, Al^{3+}, and Zn^{2+}, was evaluated by ultraviolet–visible (UV–Vis) spectrometry. As shown in Fig. 4, the spectrum of **7c** was significantly changed upon the addition of $CuCl_2$, $AlCl_3$ and $FeSO_4$. The maximum absorption at 310 nm shifted to 304 nm, 303 nm and 308 nm, respectively, and the absorption decreased, which indicated a possible interaction between these biometals and **7c**. However, no remarkable shift was observed upon the addition of $ZnCl_2$.

To determine the stoichiometry of the **7c**-Cu^{2+} complex, the molar ratio method was measured by preparing solutions of target compound **7c** with increasing amounts of $CuCl_2$. The absorbance of the **7c** complex at corresponding concentrations at 304 nm was obtained by using the UV spectra. As shown in Fig. 5, the absorbance linearly increased at first, and then it plateaued when the mole fraction of Cu^{2+} to **7c** was about 0.98, demonstrating a 1:1 stoichiometry for complex **7c**-Cu^{2+}.

2.2.6. Inhibition of self- and Cu^{2+}-induced $A\beta_{1-42}$ aggregation

The inhibitory activities of self- and Cu^{2+}-induced $A\beta_{1-42}$ aggregation of our title compounds were determined by a thioflavin T fluorescence method, with curumin as reference compound [44,45]. The results were displayed in Table 3. It indicated that these derivatives exhibited poor to moderate inhibitory activities of self- and Cu^{2+}-induced $A\beta_{1-42}$ aggregation (10.5–68.3% and 11.8–61.5% at 25 μM, respectively) with the exception of compounds **7j** and **23**. In generally, the benzylamine substituted compounds possessed higher $A\beta_{1-42}$ aggregation inhibitory activities than the aliphatic amine substituted compounds. In particular, compounds **7c**, **7l**, **7m** and **7n** were the most potent self-induced $A\beta_{1-42}$ aggregation inhibitors among all these compounds with inhibition ratios of 55.0%, 56.6%, 62.4% and 68.3% at 25 μM, respectively. Moreover, compound **13b** displayed the most potent inhibition effect on Cu^{2+}-induced $A\beta_{1-42}$ aggregation with the percentage of 61.5%. Noticeably, compounds **22–24** all displayed poor inhibitory activity of Cu^{2+}-induced $A\beta_{1-42}$ aggregation, indicating the introduction of amido bond might have adverse impact to their activities against $A\beta_{1-42}$ aggregation, compared with that of compound **7a** (34.2%).

2.2.7. Recombinant human MAO-A and -B inhibition studies

To further assess the multi-potent biological profile of target compounds, the inhibitory activity against recombinant human MAO-A and -B was measured by a fluorimetric method with kynuramine as a common substrate [46]. Clorgyline, rasagiline and iproniazid were used as reference compounds. As shown in Table 3, most of the derivatives could effectively inhibit MAO-B with IC_{50} ranging from mircomolar to submicromolar. Interestingly, almost the compounds showed poor MAO-A inhibition activity, indicating that most of the compounds are excellent selective MAO-B inhibitors. From the results of **7c**, **7d**, **15a** and **15b**, we could find that the MAO-B inhibitory potency was closely related to the amine moiety substituted position. In particular, compound **22–24** displayed decreased trend of the inhibitory potency compared to **7a**, indicating the chalcone skeleton was more appropriate for the MAO-B inhibitory potency.

2.2.8. Molecular modeling studies of MAOs

Docking simulations were performed to explore the hypothetical binding modes of the target compounds with respect to both isoforms of human MAOs. Taking into account the results of the above assays, compound **7c** was selected as the optimal representative compound for the docking studies based on the X-ray crystal structures of human MAO-A (PDB code: *2Z5X*) and MAO-B (PDB code: *2 V60*) [47]. The most stable binding modes of **7c** in hMAO-A and -B active sites were graphically inspected (Fig. 6). As shown in Fig. 6**A**, the A ring of **7c** was

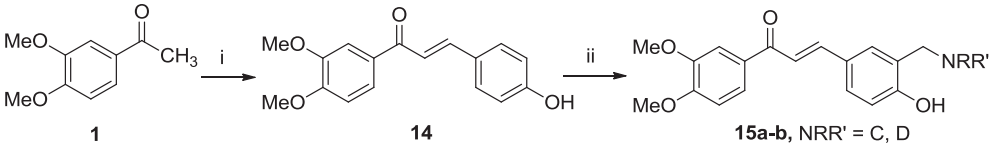

Scheme 4. Synthesis of 4′–OH chalcone Mannich base **15a-b**. *Reagents and conditions:* (i) *p*-hydroxybenzaldehyde, 50% KOH, EtOH, r.t., 4 h; (ii) paraformaldehyde, secondary amine (HNRR′), EtOH, reflux for 24 h.

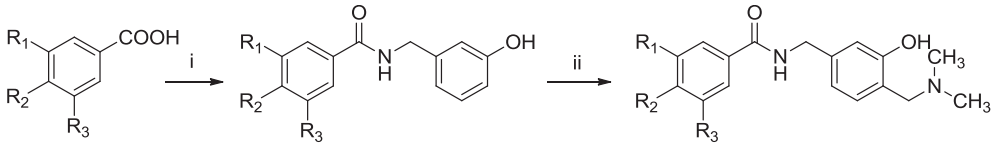

16, $R_1 = R_3 = H$, $R_2 = OMe$
17, $R_1 = R_2 = OMe$, $R_3 = H$
18, $R_1 = R_2 = R_3 = OMe$
19, $R_1 = R_3 = H$, $R_2 = OMe$
20, $R_1 = R_2 = OMe$, $R_3 = H$
21, $R_1 = R_2 = R_3 = OMe$
22, $R_1 = R_3 = H$, $R_2 = OMe$
23, $R_1 = R_2 = OMe$, $R_3 = H$
24, $R_1 = R_2 = R_3 = OMe$

Scheme 5. Synthesis of benzoyl benzylamine Mannich base **22–24**. *Reagents and conditions:* (i) EDCI, HOBt, $N(C_2H_5)_3$, 3-(aminomethyl)phenol, THF, r.t., 24 h; (ii) paraformaldehyde, dimethylamine hydrochloride, EtOH, reflux for 24–48 h.

Table 1
Chemical structures of chalcone Mannich base derivatives.

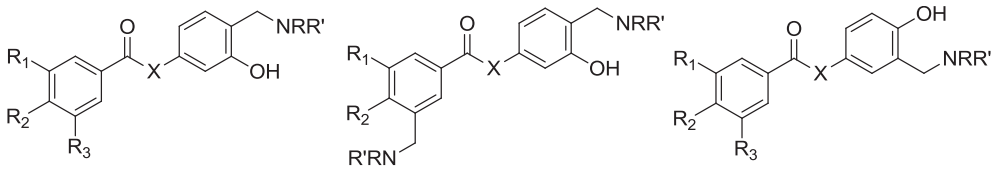

7-11, 22-24 **13a, 13b** **15a, 15b**

Compd.	X	R_1	R_2	R_3	NRR′
7a	CH = CH	OMe	OMe	H	A
7b	CH = CH	OMe	OMe	H	B
7c	CH = CH	OMe	OMe	H	C
7d	CH = CH	OMe	OMe	H	D
7e	CH = CH	OMe	OMe	H	E
7f	CH = CH	OMe	OMe	H	F
7g	CH = CH	OMe	OMe	H	G
7h	CH = CH	OMe	OMe	H	H
7i	CH = CH	OMe	OMe	H	I
7j	CH = CH	OMe	OMe	H	J
7k	CH = CH	OMe	OMe	H	K
7l	CH = CH	OMe	OMe	H	L
7m	CH = CH	OMe	OMe	H	M
7n	CH = CH	OMe	OMe	H	N
8a	CH = CH	OMe	H	H	C
8b	CH = CH	OMe	H	H	D
9a	CH = CH	H	OMe	H	C
9b	CH = CH	H	OMe	H	D
10a	CH = CH	OMe	OH	H	C
10b	CH = CH	OMe	OH	H	D
11	CH_2CH_2	OMe	OMe	H	D
13a	CH = CH	OMe	OH	—	C
13b	CH = CH	OMe	OH	—	D
15a	CH = CH	OMe	OMe	H	C
15b	CH = CH	OMe	OMe	H	D
22	$NHCH_2$	H	OMe	H	A
23	$NHCH_2$	OMe	OMe	H	A
24	$NHCH_2$	OMe	OMe	OMe	A

located far from the enzymatic cofactor FAD and no hydrogen bond or parallel π-π interaction was observed between the ligand and the active site, which explained the poor MAO-A inhibitory activities of these derivatives. However, in MAO-B docking simulation (Fig. 6**B**), the A ring of **7c** was close to the FAD cofactor. Two hydrogen bonds were generated between the ligand **7c** and the active site of MAO-B: one between the 4-carbonyl group and Tyr435 (**7c**-C═O···HO-Tyr435) and the other one between the 3′-OH group and Ile199 (**7c**-OH···O═Ile199). And the A ring of **7c** was observed to adopt a parallel π-π interaction with Tyr398. Meanwhile, other interactions could be observed between **7c** and Pro102, Pro104, Trp119, Leu167, Leu164, Phe168, Leu171, Cys172, Ile198, Ile316, Tyr326, Phe343, Phe168 and so on. Thus, the docking studies explained the high MAO-B inhibitory activity and selectivity of our derivatives.

2.2.9. *In vitro blood–brain barrier permeation assay*

The ability of a drug to cross the blood brain barrier (BBB) and penetrate into the brain is essential for successful CNS drugs. To predict the brain penetration of **7c**, the parallel artificial membrane permeation assay of the blood-brain barrier (PAMPA-BBB) was performed as reported [48]. First, we compared the permeability of 11 commercial drugs with reported values to validate the assay (Supplementary Material, Table S1). A plot of experimental data versus reported values gave a good linear correlation, P_e (exp.) = 0.9163 × P_e (bibl.) − 0.2247 (R^2 = 0.9558) (Supplementary Material, **Fig. S1**). From this equation and in view of the limit established by Di *et al.* for BBB permeation, it can be concluded that compounds with P_e values overtopping 3.44×10^{-6} cm/s could cross the blood-brain barrier (Supplementary Material, Table S2). From the measured permeability, the results showed in Table 4 indicated that compound **7c** could penetrate into the CNS with good BBB permeability.

3. Conclusion

In summary, a series of novel chalcone Mannich base derivatives were designed, synthesized and evaluated as multifunctional agents for

Table 2
Inhibition of AChE and BuChE activity, and oxygen radical absorbance capacity (ORAC, Trolox Equivalents) by chalcone Mannich base derivatives and donepezil.

Compd.	IC_{50}(μM) ± SD[a] *Ee*AChE[b]	BuChE[c] Inhibition (%)	ORAC[d]
7a	2.62 ± 0.56	n.a.[e]	1.99 ± 0.33
7b	0.89 ± 0.03	n.a.[e]	2.21 ± 0.25
7c	0.44 ± 0.04	n.a.[e]	1.93 ± 0.07
7d	0.49 ± 0.02	6.39 ± 0.67	1.34 ± 0.11
7e	9.12 ± 0.83	n.a.[e]	1.76 ± 0.08
7f	0.88 ± 0.03	22.20 ± 0.89	1.89 ± 0.06
7g	30.23 ± 3.57	n.a.[e]	1.81 ± 0.08
7h	73.64 ± 7.73	n.a.[e]	1.76 ± 0.03
7i	n.a.[e]	n.a.[e]	0.99 ± 0.05
7j	43.02 ± 3.78	n.a.[e]	1.31 ± 0.13
7k	37.05 ± 2.69	6.83 ± 0.33	1.49 ± 0.06
7l	35.96 ± 1.58	13.23 ± 1.00	1.56 ± 0.02
7m	27.43 ± 2.35	9.12 ± 0.83	1.69 ± 0.02
7n	> 200	n.a.[e]	1.86 ± 0.03
8a	0.37 ± 0.02	8.92 ± 0.63	1.51 ± 0.05
8b	4.79 ± 0.67	19.4 ± 1.23	1.17 ± 0.03
9a	0.56 ± 0.04	19.7 ± 1.13	1.28 ± 0.01
9b	1.66 ± 0.08	6.55 ± 0.23	1.19 ± 0.02
10a	0.92 ± 0.03	n.a.[e]	0.96 ± 0.01
10b	3.01 ± 0.05	n.a.[e]	1.13 ± 0.03
11	0.30 ± 0.01	29.2 ± 1.20	1.27 ± 0.04
13a	0.07 ± 0.01	n.a.[e]	1.31 ± 0.05
13b	0.18 ± 0.03	n.a.[e]	0.82 ± 0.01
15a	38.7 ± 1.08	n.a.[e]	1.74 ± 0.09
15b	24.3 ± 0.89	n.a.[e]	1.36 ± 0.05
22	> 200	n.a.[e]	1.88 ± 0.06
23	46.54 ± 2.78	n.a.[e]	2.04 ± 0.13
24	29.73 ± 1.23	n.a.[e]	2.15 ± 0.16
4	42.23 ± 1.64	n.a.[e]	1.52 ± 0.02
Donepezil	0.12 ± 0.01	IC_{50} = 20.7 ± 1.36 μM	n.t.[f]

[a] Values are expressed as the mean ± standard deviation of the mean of three independent experiments.
[b] From *Electrophorus electricus*.
[c] BuChE from rat serum was used and tested compounds were used at 50 mM.
[d] Results are expressed as μM of Trolox equivalent/μM of tested compound.
[e] n.a. = not active. It represents compounds with percent inhibition of less than 5.0% at a concentration of 50 μM in the experiment conditions.
[f] n.t. = not tested.

the treatment of AD. *In vitro* assays demonstrated that most of them exerted potent selective inhibition toward AChE, significant MAO-B inhibitions, good antioxidant activities, moderate inhibitory activities of self- and Cu^{2+}-induced $A\beta_{1-42}$ aggregation. Among these compounds, **7c** exhibited moderate inhibitory potency against AChE in the submicromolar range (IC_{50} = 0.44 μM) and against MAO-B in micromolar range (IC_{50} = 1.21 μM), good inhibitory effect of self-induced $A\beta_{1-42}$ aggregation (55.0%, at 25 μM), biometal chelating property, and moderate antioxidant activity with a value 1.93-fold of Trolox. Moreover, both kinetic analysis of AChE inhibition and molecular modeling study suggested that **7c** showed a mixed-type inhibition and binding simultaneously to CAS and PAS of AChE. Further studies indicated that **7c** showed high BBB permeability. Overall, these properties highlighted that compound **7c** might be a potential multifunctional agent for the treatment of AD and offered a starting point for design of new multitarget AChE/MAO-B inhibitors based on chalcone scaffold.

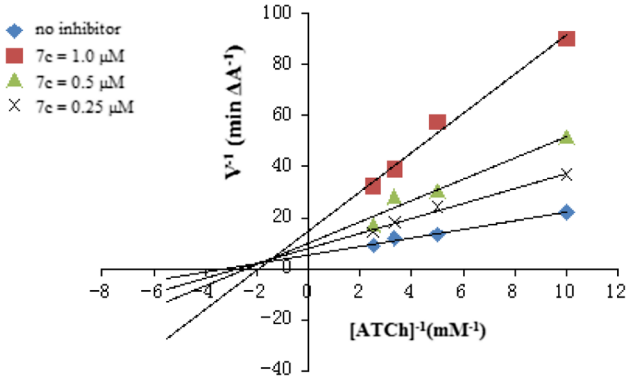

Fig. 2. Kinetic study on the mechanism of *Ee*AChE inhibition by compound **7c**. Merged Lineweaver-Burk reciprocal plots of AChE initial velocity with increasing substrate concentration (0.1–0.4 mM) in the absence or presence of **7c**. Lines were derived from a weighted least-squares analysis of data points.

4. Experimental section

4.1. Chemistry

Unless otherwise noted, all of the materials and reagents were obtained commercially and used without further purification. Melting points (uncorrected) were recorded on YRT-3 melting-point apparatus (China). ^{1}H NMR and ^{13}C NMR spectra were recorded using TMS (Tetramethylsilicane) as the internal standard at the temperature in $CDCl_3$ with a Varian INOVA 400 or 600 NMR spectrometer. Chemical shifts are reported in parts per millions (ppm) relative to TMS and the coupling constants in Hz. Mass spectra were recorded on Agilent-6210 TOF LC-MS Spectrometer. All the air sensitive reactions were performed under argon, and monitored by thin-layer chromatography (TLC) on silica gel GF254 plates from Qingdao Haiyang Chemical Co. Ltd. (China), and spots were visualized in an iodine chamber or with an UV light(254 nm). Column chromatography was performed on silica gel (230–400 mesh) purchased from Qingdao Haiyang Chemical Co.Ltd (China).

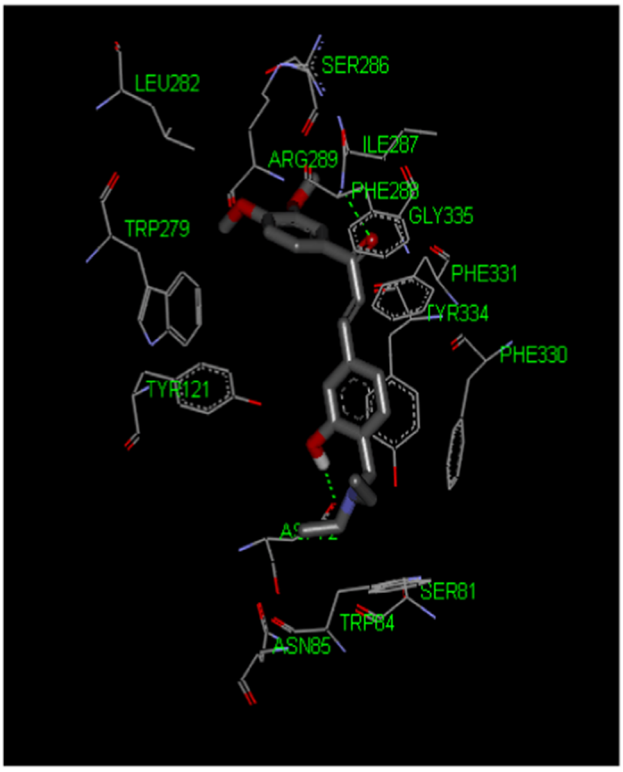

Fig. 3. Docking model of compound **7c** (colored by atom type) interacting with residues in the binding site of *Tc*AChE (PDB code: *1EVE*), the protein residues that participate in the main interactions with the inhibitor are labeled.

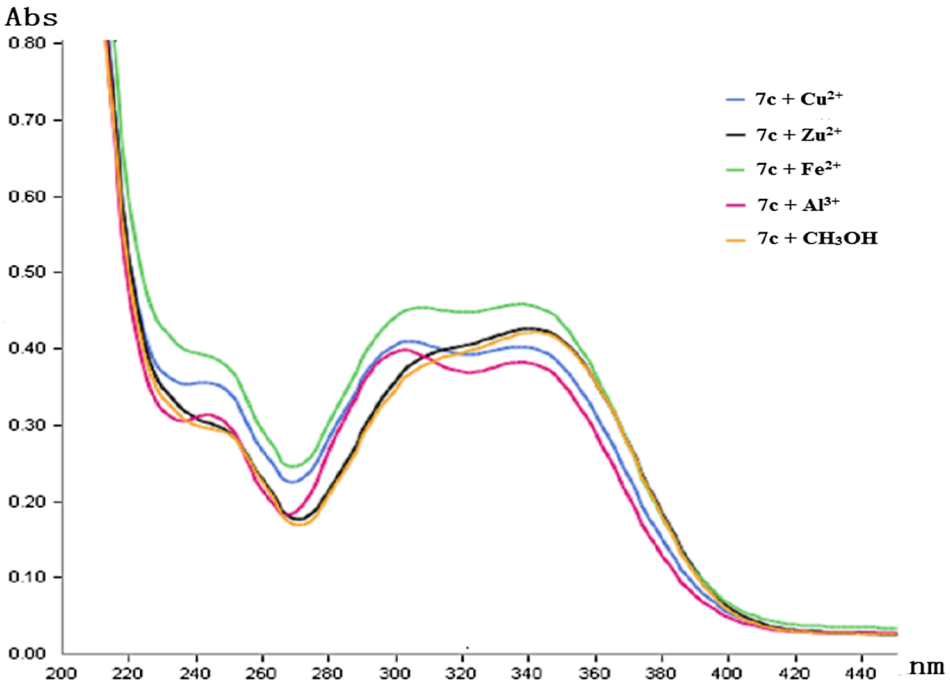

Fig. 4. UV spectrum of compound **7c** (37.5 μM in methanol) alone or in the presence of $CuCl_2$, $FeSO_4$, $ZnCl_2$ or $AlCl_3$ (37.5 μM for all metals in methanol).

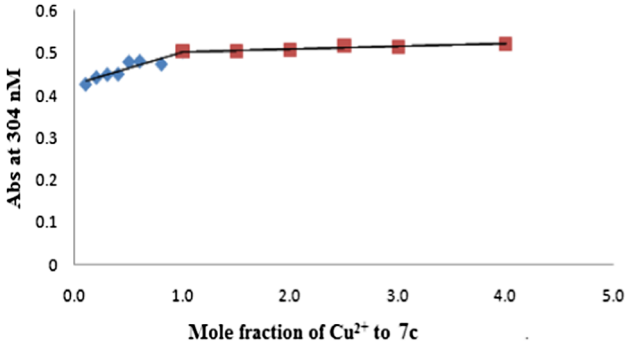

Fig. 5. Determination of the stoichiometry of complex-Cu^{2+} by using the molar ratio method of titrating the methanol solution of compound **7c** with ascending amounts of $CuCl_2$. The final concentration of **7c** was 37.5 μM, and the final concentration of Cu^{2+} ranged from 3.75 μM to 150 μM.

*4.1.1. General procedure for the synthesis of **4–6** and **14***

To a mixture of substituted benzaldehydes (6.10 mmol) and substituted acetophenones (5.55 mmol) in ethanol (15 mL) was slowly added an aqueous solution of KOH (50%, 62 mL), and stirred vigorously under an argon atmosphere at room temperature for 4–24 h. Ethanol was removed under reduced pressure. The residue was diluted in ice water and acidified with an aqueous solution of hydrochloric acid (10%), filtered and washed with water. The crude product was recrystallized with ethanol to afford the corresponding intermediates **4–6** and **14**.

*4.1.1.1. (E)-1-(3, 4-dimethoxyphenyl)-3-(3-hydroxyphenyl)prop-2-en-1-one **(4)***. It was obtained from 1-(3,4-dimethoxyphenyl)ethanone (**1**) and *m*-hydroxybenzaldehyde according to the general procedure and gave compound **4** as a yellow solid; 99.0% yield; mp 116.5–118.2 °C; (lit., [34] 113–115 °C).

*4.1.1.2. (E)-3-(3-hydroxyphenyl)-1-(3-methoxyphenyl)prop-2-en-1-one **(5)***. It was obtained from 1-(3-methoxyphenyl)ethanone (**2**) and *m*-hydroxybenzaldehyde according to the general procedure and gave compound **5** as a light red solid ; 85.2% yield; mp 98–100 °C; (lit., [35] 99–101 °C).

*4.1.1.3. (E)-3-(3-hydroxyphenyl)-1-(4-methoxyphenyl)prop-2-en-1-one **(6)***. It was obtained from 1-(4-methoxyphenyl)ethanone (**3**) and *m*-hydroxybenzaldehyde according to the general procedure and gave compound **6** as a light yellow solid; 91.5% yield; mp 162–163 °C; (lit., [36] 163–164 °C).

*4.1.1.4. (E)-1-(3,4-dimethoxyphenyl)-3-(4-hydroxyphenyl)prop-2-en-1-one **(14)***. It was obtained from 1-(3,4-dimethoxyphenyl)ethanone (**1**) and *p*-hydroxybenzaldehyde according to the general procedure and gave compound **14** as a yellow solid; 88.5% yield; mp 146–147 °C; (lit., [37] 148–149 °C).

*4.1.2. General procedure for the synthesis of **7a-n**, **8a-b**, **9a-b** and **15a-b***

The mixture of secondary amine (0.77 mmol) and paraformaldehyde (0.77 mmol) in ethanol was refluxed for 1 h, until paraformaldehyde was dissolved. Chalcone intermediates (**4–6**, **14**) (0.39 mmol) were then added in one portion. The reaction mixture was refluxed for 24–48 h. Ethanol was then removed under vacuum. The residue was diluted with water and extracted with dichloromethane (10 mL × 3). The combined organic phases were washed with saturated aqueous sodium chloride, dried over sodium sulfate, filtered and concentrated under reduced pressure. The residue was purified on a silica gel chromatography using mixtures of petroleum ether/ethyl acetate (3:1) as eluent to give corresponding target compounds **7a-n**, **8a-b**, **9a-b** and **15a-b**.

*4.1.2.1. (E)-1-(3,4-dimethoxyphenyl)-3-(4-((dimethylamino)methyl)-3-hydroxphenyl)prop-2-en-1-one **(7a)***. It was obtained from **4** and dimethylamine hydrochloride according to the general procedure and gave compound **7a** as a yellow solid; 51.0% yield; mp 51.7–53.5 °C; ^{1}H NMR (400 MHz, $CDCl_3$) δ 7.77 (d, J = 15.6 Hz, 1H), 7.68 (d, J = 8.0 Hz, 1H), 7.62 (s, 1H), 7.53 (d, J = 15.6 Hz, 1H), 7.17 (s, 1H), 7.06–7.00 (m, 2H), 6.93 (d, J = 8.0 Hz, 1H), 3.98 (s, 6H), 3.70 (s, 2H), 2.37 (s, 6H); ^{13}C NMR (150 MHz, $CDCl_3$) δ 188.4, 158.3, 153.1, 149.1, 143.8, 135.6, 131.2, 128.8, 124.4, 122.9, 121.3, 120.0, 114.7, 110.6, 109.9, 62.3, 56.0, 55.9, 44.3; ESI-MS: 342.2 $[M + H]^+$.

Table 3
Inhibition of self- and Cu^{2+}-induced $A\beta_{1-42}$ aggregation and MAO inhibitory activities of title compounds and reference compounds.

Compd.	% inhibition of Aβ aggregation[a]		MAO-A[d,e] (% inhibition)	MAO-B[e] IC_{50}(μM) ± SD
	self-induced[b,e]	Cu^{2+}-induced[c,e]		
7a	29.3 ± 0.8	34.2 ± 1.1	19.5 ± 0.6%	0.16 ± 0.02
7b	25.0 ± 1.0	24.4 ± 0.9	25.3 ± 1.0%	0.28 ± 0.01
7c	55.0 ± 1.2	20.2 ± 0.8	19.3 ± 0.6%	1.21 ± 0.03
7d	39.8 ± 1.1	11.8 ± 0.8	17.7 ± 0.7%	1.68 ± 0.03
7e	23.3 ± 0.7	13.0 ± 0.5	21.8 ± 0.9%	1.11 ± 0.04
7f	17.8 ± 0.7	20.9 ± 0.9	22.8 ± 0.6%	0.34 ± 0.01
7g	19.1 ± 0.6	14.7 ± 0.8	20.0 ± 0.6%	0.61 ± 0.02
7h	39.9 ± 1.2	27.7 ± 0.6	19.1 ± 0.7%	0.28 ± 0.01
7i	14.3 ± 0.9	30.0 ± 1.0	31.1 ± 0.8%	0.36 ± 0.02
7j	n.a.[g]	29.6 ± 1.0	22.6 ± 0.9%	0.35 ± 0.01
7k	35.8 ± 1.3	29.3 ± 1.1	23.3 ± 0.6%	0.21 ± 0.01
7l	56.6 ± 1.4	28.0 ± 0.9	21.4 ± 0.6%	0.31 ± 0.02
7m	62.4 ± 1.5	48.1 ± 1.2	30.0 ± 1.1%	0.14 ± 0.01
7n	68.3 ± 1.3	37.4 ± 1.0	23.3 ± 0.6%	0.32 ± 0.02
8a	18.9 ± 0.9	29.9 ± 0.8	63.4 ± 1.3%	0.16 ± 0.01
8b	21.2 ± 1.0	34.5 ± 0.7	33.7 ± 1.3%	0.23 ± 0.01
9a	24.2 ± 1.0	45.5 ± 1.0	54.1 ± 1.4%	0.29 ± 0.02
9b	32.8 ± 0.8	45.0 ± 1.2	42.3 ± 1.5%	1.07 ± 0.04
10a	28.9 ± 1.3	16.1 ± 0.9	45.0 ± 1.3%	42.5 ± 1.5%[d]
10b	34.8 ± 1.2	56.9 ± 1.4	27.6 ± 0.6%	1.1 ± 0.3
11	9.0 ± 0.7	45.5 ± 1.2	2.7 ± 0.4%	2.24 ± 0.4
13a	27.6 ± 0.7	52.4 ± 0.9	33.1 ± 0.6%	1.3 ± 0.3
13b	31.3 ± 1.2	61.5 ± 1.1	32.0 ± 0.8%	47.0 ± 1.3%[d]
15a	10.7 ± 0.6	38.0 ± 1.3	21.5 ± 0.6%	6.87 ± 0.2
15b	11.8 ± 0.7	35.9 ± 1.1	21.9 ± 0.6%	18.9 ± 0.5
22	10.5 ± 0.9	5.3 ± 0.5	20.6 ± 0.5%	9.4 ± 0.7%[d]
23	n.a.[g]	n.a.[g]	17.6 ± 0.9%	8.4 ± 0.5%[d]
24	23.1 ± 1.1	12.3 ± 0.9	3.8 ± 0.7%	3.5 ± 0.6%[d]
4	26.5 ± 1.0	16.3 ± 0.9	19.3 ± 0.5%	1.55 ± 0.2
Curumin	51.6 ± 0.9	67.2 ± 1.3	n.t.[f]	n.t.[f]
Clorgyline	n.t.[f]	n.t.[f]	IC_{50} = 0.0027 ± 0.0006	4.19 ± 0.101
Rasagiline	n.t.[f]	n.t.[f]	IC_{50} = 1.42 ± 0.015	0.0825 ± 0.002
Iproniazid	n.t.[f]	n.t.[f]	IC_{50} = 2.56 ± 0.023	1.95 ± 0.074

[a] For Inhibition of Aβ aggregation, the thioflavin-T fluorescence method was used.
[b] Inhibition of self-induced $A\beta_{1-42}$ aggregation (25 μM) by tested inhibitors at 25 μM.
[c] Inhibition of Cu^{2+}-induced $A\beta_{1-42}$ aggregation. The concentration of tested compounds and Cu^{2+} were 25 μM.
[d] Percentages are the percent inhibition of MAO by tested compounds at 10 μM.
[e] The mean ± SD of the three independent experiments.
[f] n.t. = not tested
[g] n.a. = not active.

*4.1.2.2. (E)-1-(3,4-dimethoxyphenyl)-3-(4-((ethyl(methyl)amino) methyl)-3-hydroxyphenyl)prop-2-en- 1-one (**7b**).* It was obtained from **4** and *N*-methylethanamine according to the general procedure and gave compound **7b** as a yellow solid; 45.0% yield; mp 51.6–52.8 °C; ^{1}H NMR (400 MHz, $CDCl_3$) δ 7.74 (d, J = 15.6 Hz, 1H), 7.68 (dd, J = 8.4, 1.6 Hz, 1H), 7.62 (s, 1H), 7.52 (d, J = 15.6 Hz, 1H), 7.16 (s, 1H), 7.06–7.01 (m, 2H), 6.94 (d, J = 8.4 Hz, 1H), 3.97 (s, 6H), 3.77 (s, 2H), 2.60 (q, J = 7.2 Hz, 2H), 2.34 (s, 3H), 1.18 (t, J = 7.2 Hz, 3H); ^{13}C NMR (150 MHz, $CDCl_3$) δ 188.4, 158.2, 153.0, 149.0, 143.7, 135.7, 131.1, 129.1, 123.8, 122.9, 121.3, 120.0, 114.8, 110.5, 109.8, 59.7, 55.9, 55.8, 50.5, 40.4, 11.6; ESI-MS: 356.2 $[M + H]^+$.

*4.1.2.3. (E)-3-(4-((diethylamino)methyl)-3-hydroxyphenyl)-1-(3,4-dimethoxyphenyl)prop-2-en-1-one (**7c**).* It was obtained from **4** and

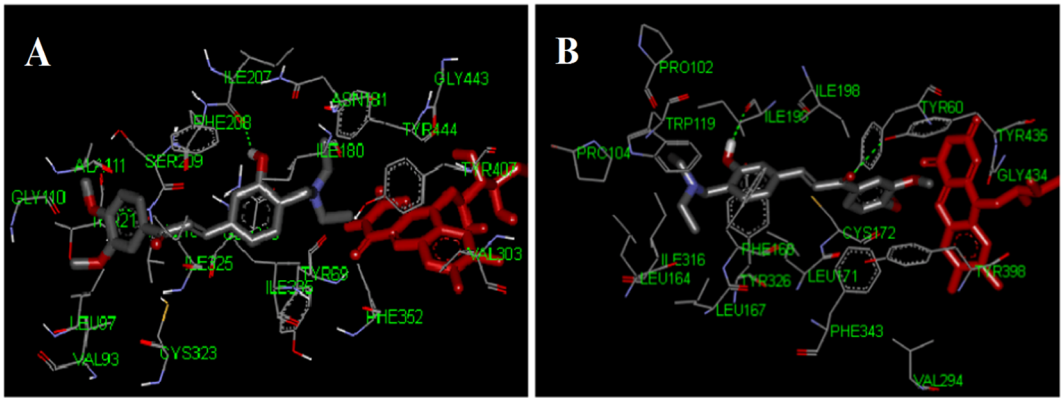

Fig. 6. Representation of compound **7c** docked into the binding sites of hMAO-A (A) and -B (B), highlighting the protein residues that participate in the main interactions with the inhibitor. Ligand **7c** and FAD are displayed in grey and red respectively. Hydrogen-bonds are shown with the green dotted lines.

Table 4
Permeability results P_e ($\times 10^{-6}$ cm/s) from the PAMPA-BBB assay for **7c** with the predicted penetration into the CNS.

Compd.[a]	P_e ($\times 10^{-6}$ cm/s)[b]	Prediction
7c	13.5 ± 0.4	CNS +

[a] Compound **7c** was dissolved in DMSO at 5 mg/mL and diluted with PBS/EtOH (70:30). The final concentration of the compound was 100 μg/mL.
[b] Data are the mean ± SD of three independent experiments.

diethylamine according to the general procedure and gave compound **7c** as a yellow oil; 46.0% yield; ^{1}H NMR (400 MHz, $CDCl_3$) δ 7.73 (d, J = 15.6 Hz, 1H), 7.68 (d, J = 8.4 Hz, 1H), 7.62 (s, 1H), 7.52 (d, J = 15.6 Hz, 1H), 7.17 (s, 1H), 7.04 (s, 2H), 6.93 (d, 1H), 3.97 (s, 6H), 3.84 (s, 2H), 2.69 (q, J = 7.6 Hz, 4H), 1.15 (t, J = 7.6 Hz, 6H); ^{13}C NMR (150 MHz, $CDCl_3$) δ 188.4, 158.5, 153.0, 149.0, 143.9, 135.4, 131.2, 128.7, 124.7, 122.8, 121.1, 119.9, 114.7, 110.6, 109.9, 56.5, 55.9, 55.8, 46.3, 10.9; ESI-MS: 370.2 $[M + H]^+$.

*4.1.2.4. (E)-1-(3,4-dimethoxyphenyl)-3-(3-hydroxy-4-(piperidin-1-ylmethyl)phenyl)prop-2-en-1-one (**7d**).* It was obtained from **4** and piperidine according to the general procedure and gave compound **7d** as a yellow solid; 50.0% yield; mp 61.4–62.5 °C; ^{1}H NMR (400 MHz, $CDCl_3$) δ 7.73 (d, J = 15.6 Hz, 1H), 7.68 (d, J = 8.4 Hz, 1H) 7.61 (s, 1H), 7.52 (d, J = 15.6 Hz, 1H), 7.20 (s, 1H), 7.02 (s, 2H), 6.93 (d, J = 8.0 Hz, 1H), 3.97 (s, 6H), 3.79 (s, 2H), 3.16 (brs, 4H), 1.71 (brs, 4H), 1.54 (brs, 2H); ^{13}C NMR (100 MHz, $CDCl_3$) δ 188.5, 158.2, 153.1, 149.0, 143.7, 135.7, 131.2, 129.3, 123.6, 122.9, 121.3, 120.0, 114.8, 110.5, 109.8, 61.1, 56.0, 55.9, 53.6, 25.3, 23.5; ESI-MS: 382.2 $[M + H]^+$.

*4.1.2.5. (E)-1-(3,4-dimethoxyphenyl)-3-(3-hydroxy-4-(morpholinomethyl)phenyl)prop-2-en-1-one (**7e**).* It was obtained from **4** and morpholine according to the general procedure and gave compound **7e** as a yellow solid; 46.0% yield; mp 56.3–57.5 °C; ^{1}H NMR (400 MHz, $CDCl_3$) δ 7.74 (d, J = 15.6 Hz, 1H), 7.68 (dd, J = 8.4, 1.6 Hz, 1H), 7.62 (d, J = 1.6 Hz, 1H), 7.52 (d, J = 15.6 Hz, 1H), 7.16 (s, 1H), 7.07–7.05 (m, 2H), 6.93 (d, J = 8.4 Hz, 1H), 3.97 (s, 6H), 3.78 (s, 2H), 3.76 (s, 4H), 2.61 (brs, 4H); ^{13}C NMR (150 MHz, $CDCl_3$) δ 188.4, 157.7, 153.1, 149.1, 143.5, 135.9, 131.2, 129.2, 123.1, 122.9, 121.4, 120.2, 114.8, 110.6, 109.8, 66.5, 61.4, 56.0, 55.9, 52.8; ESI-MS: 384.2 $[M + H]^+$.

*4.1.2.6. (E)-1-(3,4-dimethoxyphenyl)-3-(3-hydroxy-4-(pyrrolidin-1-ylmethyl)phenyl)prop-2-en-1-one (**7f**).* It was obtained from **4** and pyrrolidine according to the general procedure and gave compound **7f** as a yellow solid; 55.0% yield; mp 46.2–47.4 °C; ^{1}H NMR (400 MHz, $CDCl_3$) δ 7.72 (d, J = 15.6 Hz, 1H), 7.68 (dd, J = 8.4, 1.6 Hz, 1H), 7.61 (d, J = 1.6 Hz, 1H), 7.52 (d, J = 15.6 Hz, 1H), 7.22 (s, 1H), 7.10–7.04 (m, 2H, Ar-H), 6.93 (d, J = 8.0 Hz, 1H), 3.97 (s, 6H), 3.93 (s, 2H), 2.77 (brs, 4H), 1.91 (brs, 4H); ^{13}C NMR (100 MHz, $CDCl_3$) δ 188.5, 158.1, 153.1, 149.0, 143.8, 135.6, 131.2, 128.6, 124.5, 122.9, 121.3, 120.0, 114.7, 110.5, 109.8, 57.9, 56.0, 55.9, 53.3, 23.5; ESI-MS: 368.2 $[M + H]^+$.

*4.1.2.7. (E)-1-(3,4-dimethoxyphenyl)-3-(3-hydroxy-4-((4-methylpiperazin-1-yl)methyl)phenyl)prop-2- en-1-one (**7g**).* It was obtained from **4** and *N*-methylpiperazine according to the general procedure and gave compound **7g** as a yellow solid; 57.0% yield; mp 57.2–58.5 °C; ^{1}H NMR (400 MHz, $CDCl_3$) δ 7.74 (d, J = 15.6 Hz, 1H), 7.68 (d, J = 8.4 Hz, 1H), 7.62 (s, 1H), 7.52 (d, J = 15.6 Hz, 1H), 7.14 (s, 1H), 7.07–7.02 (m, 2H), 6.93 (d, J = 8.4 Hz, 1H), 3.97 (s, 6H), 3.76 (s, 2H), 2.51 (brs, 8H), 2.32 (s, 3H); ^{13}C NMR (100 MHz, $CDCl_3$) δ 188.3, 157.8, 153.0, 149.0, 143.6, 135.6, 131.1, 129.0, 123.6, 122.8, 121.2, 120.0, 114.7, 110.5, 109.8, 60.9, 55.9, 55.8, 54.6, 52.3, 45.6; ESI-MS: 397.2 $[M + H]^+$.

*4.1.2.8. (E)-1-(3,4-dimethoxyphenyl)-3-(4-((4-ethylpiperazin-1-yl) methyl)-3-hydroxyphenyl)prop-2- en-1-one (**7h**).* It was obtained from **4** and *N*-ethylpiperazine according to the general procedure and gave compound **7h** as a yellow solid; 70.0% yield; mp 50.5–51.6 °C; ^{1}H NMR (400 MHz, $CDCl_3$) δ 7.72 (d, J = 15.6 Hz, 1H), 7.66 (d, J = 8.4 Hz, 1H), 7.60 (s, 1H), 7.50 (d, J = 15.6 Hz, 1H), 7.12 (s, 1H), 7.05–7.00 (m, 2H), 6.92 (d, J = 8.0 Hz, 1H), 3.96 (s, 6H), 3.74 (s, 2H), 2.61 (brs, 8H), 2.44 (q, J = 6.8 Hz, 2H), 1.08 (t, J = 6.8 Hz, 3H); ^{13}C NMR (150 MHz, $CDCl_3$) δ 188.3, 157.9, 153.0, 149.0, 143.6, 135.6, 131.2, 129.0, 123.7, 122.8, 121.2, 120.0, 114.7, 110.5, 109.8, 61.0, 55.9, 55.9, 55.8, 52.3, 51.9, 11.7; ESI-MS: 411.2 $[M + H]^+$.

*4.1.2.9. (E)-3-(4-((4-benzylpiperazin-1-yl)methyl)-3-hydroxyphenyl)-1-(3,4-dimethoxyphenyl)prop-2- en-1-one (**7i**).* It was obtained from **4** and *N*-benzylpiperazine according to the general procedure and gave compound **7i** as a yellow solid; 51.0% yield; mp 57.3–58.5 °C; ^{1}H NMR (400 MHz, $CDCl_3$) δ 7.72 (d, J = 15.6 Hz, 1H), 7.66 (d, J = 8.4 Hz, 1H), 7.60 (s, 1H), 7.50 (d, J = 15.6 Hz, 1H), 7.30–7.24 (m, 5H), 7.12 (s, 1H), 7.03–6.99 (m, 2H), 6.92 (d, J = 8.0 Hz, 1H), 3.96 (s, 6H), 3.74 (s, 2H), 3.53 (s, 2H), 2.58 (brs, 8H); ^{13}C NMR (150 MHz, $CDCl_3$) δ 188.5, 158.0, 153.1, 149.1, 1, 143.8, 135.7, 131.3, 129.1, 129.0, 128.2, 127.2, 123.8, 122.9, 121.3, 120.1, 114.7, 110.6, 109.9, 62.7, 61.1, 56.0, 56.0, 55.9, 52.7, 52.4; ESI-MS: 473.2 $[M + H]^+$.

*4.1.2.10. (E)-3-(4-((benzyl(ethyl)amino)methyl)-3-hydroxyphenyl)-1-(3,4-dimethoxyphenyl)prop-2- en-1-one (**7j**).* It was obtained from **4** and *N*-benzylethanamine according to the general procedure and gave compound **7j** as a yellow solid; 48.0% yield; mp 49.5–50.7 °C; ^{1}H NMR (400 MHz, $CDCl_3$) δ 7.74 (d, J = 15.6 Hz, 1H), 7.68 (d, J = 7.6 Hz, 1H), 7.62 (s, 1H), 7.51 (d, J = 15.6 Hz, 1H), 7.36–7.30 (m, 5H), 7.15 (s, 1H), 7.04 (s, 2H), 6.93 (d, J = 8.0 Hz, 1H), 3.97 (s, 6H), 3.81 (s, 2H), 3.67 (s, 2H), 2.62 (q, J = 7.2 Hz, 2H), 1.16 (t, J = 7.2 Hz, 3H); ^{13}C NMR (150 MHz, $CDCl_3$) δ 188.5, 158.2, 153.1, 149.1, 143.8, 136.5, 135.6, 131.3, 129.4, 129.0, 128.6, 127.6, 124.7, 122.9, 121.3, 120.2, 114.7, 110.6, 109.9, 57.5, 56.6, 56.0, 55.9, 46.6, 11.0; ESI-MS: 432.2 $[M + H]^+$.

*4.1.2.11. (E)-1-(3,4-dimethoxyphenyl)-3-(3-hydroxy-4-(((2-methoxybenzyl)(methyl)amino)methyl) phenyl)prop-2-en-1-one (**7k**).* It was obtained from **4** and *N*-(2-methoxybenzyl)methylamine according to the general procedure and gave compound **7k** as a yellow solid; 45.0% yield; mp 148.1–149.5 °C; ^{1}H NMR (400 MHz, $CDCl_3$) δ 7.72 (d, J = 15.6 Hz, 1H), 7.66 (d, J = 8.4 Hz, 1H), 7.60 (s, 1H), 7.50 (d, J = 15.6 Hz, 1H), 7.29 (t, J = 7.6 Hz, 1H), 7.20 (d, J = 7.6 Hz, 1H), 7.14 (s, 1H), 7.02 (s, 2H), 6.93–6.89 (m, 3H), 3.96 (s, 6H), 3.88 (s, 3H), 3.76 (s, 2H), 3.67 (s, 2H), 2.20 (s, 3H); ^{13}C NMR (150 MHz, $CDCl_3$) δ 188.5, 158.3, 158.1, 153.1, 149.1, 143.9, 135.5, 131.3, 129.3, 128.9, 125.1, 124.6, 122.9, 121.2, 120.2, 120.0, 114.7, 110.6, 110.4, 109.9, 60.3, 57.0, 56.0, 55.9, 55.1, 40.8; ESI-MS: 448.2 $[M + H]^+$.

*4.1.2.12. (E)-1-(3,4-dimethoxyphenyl)-3-(4-((ethyl(2-methoxybenzyl) amino)methyl)-3-hydroxy phenyl)prop-2-en-1-one (**7l**).* It was obtained from **4** and *N*-(2-methoxybenzyl)ethanamine according to the general procedure and gave compound **7l** as a yellow solid; 46.0% yield; mp 50.7–51.8 °C; ^{1}H NMR (400 MHz, $CDCl_3$) δ 7.71 (d, J = 15.6 Hz, 1H), 7.65 (d, J = 8.0 Hz, 1H), 7.60 (s, 1H), 7.50 (d, J = 15.6 Hz, 1H), 7.28 (t, J = 7.6 Hz, 1H), 7.21 (d, J = 7.6 Hz, 1H), 7.12 (s, 1H), 6.99 (s, 2H), 6.92–6.88 (m, 3H), 3.96 (s, 6H), 3.88 (s, 3H), 3.78 (s, 2H), 3.71(s, 2H), 2.61 (q, J = 7.2 Hz, 2H), 1.14 (t, J = 7.2 Hz, 3H); ^{13}C NMR (150 MHz, $CDCl_3$) δ 188.5, 158.3, 158.0, 153.1, 149.0, 143.9, 135.4, 131.4, 131.3, 129.3, 129.0, 122.9, 121.1, 120.2, 120.0, 114.6, 110.6, 110.5, 109.9, 56.3, 56.0, 55.9, 55.1, 52.7, 46.6, 10.5; ESI-MS: 462.2 $[M + H]^+$.

4.1.2.13. (E)-1-(3,4-dimethoxyphenyl)-3-(4-(((2-(dimethylamino)benzyl)

*(ethyl)amino)methyl)-3- hydroxyphenyl)prop-2-en-1-one (**7m**)*. It was obtained from **4** and 2-((ethylamino)methyl)-*N*,*N*-dimethylaniline according to the general procedure and gave compound **7m** as a yellow solid; 70.0% yield; mp 68.5–70.2 °C; ^{1}H NMR (400 MHz, $CDCl_3$) δ 7.75 (d, J = 15.6 Hz, 1H), 7.68 (d, J = 7.6 Hz, 1H), 7.61 (s, 1H), 7.52 (d, J = 15.6 Hz, 1H), 7.37–7.35 (m, 2H), 7.18–7.16 (m, 2H), 7.09 (brt, 1H), 7.03 (s, 2H), 6.93 (d, J = 7.6 Hz, 1H), 3.97 (s, 6H), 3.81 (s, 4H), 2.67 (s, 6H), 2.60 (brs, 2H), 1.15 (brs, 3H); ^{13}C NMR (150 MHz, $CDCl_3$) δ 188.5, 158.1, 153.3, 153.0, 149.0, 143.8, 135.5, 131.2, 130.6, 129.1, 128.5, 123.7, 122.9, 121.2, 120.0, 119.8, 114.5, 110.6, 109.9, 56.7, 56.0, 55.9, 52.9, 46.7, 45.1, 10.5; ESI-MS: 475.3 $[M + H]^+$.

*4.1.2.14. (E)-1-(3,4-dimethoxyphenyl)-3-(4-((((4-(dimethylamino)benzyl)(ethyl)amino)methyl)-3- hydroxyphenyl)prop-2-en-1-one (**7n**)*. It was obtained from **4** and 4-((ethylamino)methyl)-*N*,*N*-dimethylaniline according to the general procedure and gave compound **7n** as a yellow solid; 55.0% yield; mp 103.2–104.7 °C; ^{1}H NMR (400 MHz, $CDCl_3$) δ 7.73 (d, J = 15.6 Hz, 1H), 7.67 (d, J = 8.4 Hz, 1H), 7.62 (s, 1H), 7.51 (d, J = 15.6 Hz, 1H), 7.19–7.16 (m, 3H), 7.05–7.03 (m, 2H), 6.93 (d, J = 8.4 Hz, 1H), 6.71 (d, J = 8.8 Hz, 2H), 3.97 (s, 6H), 3.81 (s, 2H), 3.62 (s, 2H), 2.94 (s, 6H), 2.63 (q, J = 7.2 Hz, 2H), 1.17 (t, J = 7.2 Hz, 3H); ESI-MS: 475.3 $[M + H]^+$.

*4.1.2.15. (E)-3-(4-((diethylamino)methyl)-3-hydroxyphenyl)-1-(3-methoxyphenyl)prop-2-en-1-one (**8a**)*. It was obtained from **5** and diethylamine according to the general procedure and gave compound ***8a*** as a yellow oil; 50.0% yield; ^{1}H NMR (400 MHz, $CDCl_3$) δ 7.74 (d, J = 16.0 Hz, 1H), 7.59 (d, J = 8.0 Hz, 1H), 7.54 (s, 1H), 7.49 (d, J = 16.0 Hz, 1H), 7.41 (t, J = 8.0 Hz, 1H), 7.14–7.12 (m, 2H), 7.05–7.00 (m, 2H), 3.89(s, 3H), 3.81 (s, 2H), 2.65 (q, J = 7.2 Hz, 4H), 1.13 (t, J = 7.2 Hz, 6H); ESI-MS: 340.2 $[M + H]^+$.

*4.1.2.16. (E)-3-(3-hydroxy-4-(piperidin-1-ylmethyl)phenyl)-1-(3-methoxyphenyl)prop-2-en-1-one (**8b**)*. It was obtained from **5** and piperidine according to the general procedure and gave compound **8b** as a yellow solid; 51.0% yield; mp 109.5–111.3 °C; ^{1}H NMR (400 MHz, $CDCl_3$) δ 7.74 (d, J = 15.6 Hz, 1H), 7.59 (d, J = 7.6 Hz, 1H), 7.54–7.53 (m, 1H), 7.47 (d, J = 15.6 Hz, 1H), 7.41 (t, J = 8.0 Hz, 1H), 7.14–7.12 (m, 2H), 7.05–6.99 (m, 2H), 3.89 (s, 3H), 3.72 (s, 2H), 2.54 (brs, 4H), 1.68–1.65 (m, 4H), 1.51 (brs, 2H); ^{13}C NMR (150 MHz, $CDCl_3$) δ 190.2, 159.8, 158.4, 144.8, 139.6, 135.3, 129.5, 129.0, 124.5, 121.7, 120.9, 119.9, 119.3, 114.9, 112.7, 61.7, 55.4, 53.8, 25.7, 23.8; ESI-MS: 352.2 $[M + H]^+$.

*4.1.2.17. (E)-3-(4-((diethylamino)methyl)-3-hydroxyphenyl)-1-(4-methoxyphenyl)prop-2-en-1-one (**9a**)*. It was obtained from **6** and diethylamine according to the general procedure and gave compound **9a** as a yellow oil; 49.0% yield; ^{1}H NMR (400 MHz, $CDCl_3$) δ 8.03 (d, J = 8.4 Hz, 2H), 7.72 (d, J = 15.6 Hz, 1H), 7.50 (d, J = 15.6 Hz, 1H), 7.16 (s , 1H), 7.04–6.92 (m, 4H), 3.89 (s, 3H), 3.84 (s, 2H), 2.69 (q, J = 7.2 Hz, 4H), 1.16 (t, J = 7.2 Hz, 6H); ESI-MS: 340.2 $[M + H]^+$.

*4.1.2.18. (E)-3-(3-hydroxy-4-(piperidin-1-ylmethyl)phenyl)-1-(4-methoxyphenyl)prop-2-en-1-one (**9b**)*. It was obtained from **6** and piperidine according to the general procedure and gave compound **9b** as a yellow solid; 45.0% yield; mp 116.9–118.5 °C (lit [38]. mp 120–121 °C); ^{1}H NMR (400 MHz, $CDCl_3$) δ 8.03 (d, J = 8.4 Hz, 2H), 7.73 (d, J = 15.6 Hz, 1H), 7.50 (d, J = 15.6 Hz, 1H), 7.13 (s, 1H), 7.05–6.97(m, 4H), 3.89 (s, 3H), 3.72 (s, 2H), 2.66 (brs, 4H), 1.67 (brs, 4H), 1.51 (brs, 2H); ^{13}C NMR (150 MHz, $CDCl_3$) δ 188.7, 163.4, 158.4, 143.9, 135.6, 131.2, 130.8, 129.0, 124.2, 121.6, 119.9, 114.9, 113.8, 61.8, 55.5, 53.9, 25.7, 23.8; ESI-MS: 352.2 $[M + H]^+$.

*4.1.2.19. (E)-3-(3-((diethylamino)methyl)-4-hydroxyphenyl)-1-(3,4-dimethoxyphenyl)prop-2-en-1- one (**15a**)*. It was obtained from **14** and diethylamine according to the general procedure and gave compound **15a** as a yellow oil; 48.0% yield; ^{1}H NMR (600 MHz, $CDCl_3$) 7.50 (d, J = 15.6 Hz, 1H), 7.68 (d, J = 8.4 Hz, 1H), 7.63 (s, 1H), 7.51 (d, J = 8.4 Hz, 1H), 7.40 (d, J = 15.6 Hz, 1H), 7.30 (s, 1H), 6.92 (d, J = 7.8 Hz, 1H), 6.86 (d, J = 7.8 Hz, 1H), 3.97 (s, 6H), 3.85 (s, 2H), 2.69 (q, J = 4.8 Hz, 4H), 1.15 (t, J = 7.2 Hz, 6H); ^{13}C NMR (100 MHz, $CDCl_3$) δ 188.4, 161.1, 152.8, 148.9, 144.1, 131.4, 129.2, 129.1, 125.8, 122.6, 121.9, 118.1, 116.6, 110.5, 109.8, 56.2, 55.8, 46.1, 10.8; ESI-MS: 370.2 $[M + H]^+$.

*4.1.2.20. (E)-1-(3,4-dimethoxyphenyl)-3-(4-hydroxy-3-(piperidin-1-ylmethyl)phenyl)prop-2-en-1-one (**15b**)*. It was obtained from **14** and piperidine according to the general procedure and gave compound **15b** as a yellow solid; 50.5% yield; mp 57.8–58.5 °C; ^{1}H NMR (400 MHz, $CDCl_3$) δ 7.79 (d, J = 15.6 Hz, 1H), 7.68 (d, J = 7.6 Hz, 1H), 7.63 (s, 1H), 7.51 (d, J = 7.6 Hz, 1H), 7.40 (d, J = 15.6 Hz, 1H), 7.29 (s, 1H), 6.92 (d, J = 8.4 Hz, 1H), 6.86 (d, J = 8.4 Hz, 1H), 3.97(s, 6H), 3.75 (s, 2H), 2.81 (brs, 4H), 1.67 (s, 4H), 1.52 (brs, 2H); ^{13}C NMR (150 MHz, $CDCl_3$) δ 188.7, 160.9, 153.0, 149.1, 144.3, 131.6, 129.3, 129.3, 126.1, 122.8, 121.7, 118.4, 116.8, 110.7, 109.9, 61.6, 56.0, 53.8, 25.6, 23.7; ESI-MS: 382.2 $[M + H]^+$.

*4.1.3. General procedure for the synthesis of **10a-b***

A mixture of compounds **7c** or **7d** (0.26 mmol), $AlCl_3$ (1.05 mmol) in CH_2Cl_2 (2.0 mL), was stirred at room temperature for 6 h under argon atmosphere. The reaction mixture then poured into ice water and stirred for 10 min, the mixture was extracted with dichloromethane (10 mL × 3). The combined organic phases were washed with saturated aqueous sodium chloride, dried over sodium sulfate, filtered and under reduced pressure. The residue was purified on a silica gel chromatography using mixtures of petroleum ether/acetone (3:1) as eluent to give the corresponding compounds **10a-b**.

*4.1.3.1. (E)-3-(4-((diethylamino)methyl)-3-hydroxyphenyl)-1-(4-hydroxy-3-methoxyphenyl)prop-2- en-1-one (**10a**)*. It was obtained from **7c** according to the general procedure and gave compound **10a** as a yellow oil; 50% yield; ^{1}H NMR (400 MHz, $CDCl_3$) δ 7.72 (d, J = 15.6 Hz, 1H), 7.64–7.61 (m, 2H), 7.50 (d, J = 15.6 Hz, 1H), 7.14 (s, 1H), 7.03–6.98 (m, 3H), 3.97 (s, 3H), 3.83 (s, 2H), 2.67 (q, J = 7.2 Hz, 4H), 1.14 (t, J = 7.2 Hz, 6H); ESI-MS: 356.2 $[M + H]^+$.

*4.1.3.2. (E)-1-(4-hydroxy-3-methoxyphenyl)-3-(3-hydroxy-4-(piperidin-1-ylmethyl)phenyl)prop-2- en-1-one (**10b**)*. It was obtained from **7d** according to the general procedure and gave compound **10b** as a yellow solid; 48.0% yield; mp 72.5–73.8 °C; ^{1}H NMR (400 MHz, $CDCl_3$) δ 7.73 (d, J = 15.6 Hz, 1H), 7.65–7.62 (m, 2H), 7.50 (d, J = 15.6 Hz, 1H), 7.13 (s, 1H), 7.04–6.98 (m, 3H), 3.98 (s, 3H), 3.70 (s, 2H), 2.53 (brs, 4H), 1.67–1.64 (m, 4H), 1.51 (brs, 2H); ESI-MS: 368.2 $[M + H]^+$.

*4.1.4. 1-(3,4-dimethoxyphenyl)-3-(3-hydroxy-4-(piperidin-1-ylmethyl) phenyl)propan-1-one (**11**)*

A mixture of **7d** (0.42 mmol), 10% pd/C (16 mg) in THF (2.0 mL) was stirred at room temperature for 10 h under hydrogen atmosphere of about 1 atm. The reaction mixture was filtered and the filtrate was concentrated under reduced pressure. The residue was purified on a silica gel chromatography using mixtures of petroleum ether/acetone (5:1) as eluent to give compound **11** as an oil; 60.0% yield; ^{1}H NMR (400 MHz, $CDCl_3$) δ 7.59 (dd, J = 8.4, 1.6 Hz, 1H), 7.52 (s, 1H), 6.89–6.87 (m, 2H), 6.73 (s, 1H), 6.87 (d, J = 7.6 Hz, 1H), 3.94 (s, 6H), 3.67 (s, 2H), 3.23 (t, J = 7.6 Hz, 2H), 2.98 (t, J = 7.6 Hz, 2H), 2.52 (brs, 4H), 1.66–1.62 (m, 4H), 1.50 (brs, 2H). ^{13}C NMR (150 MHz, $CDCl_3$) δ 197.9, 157.9, 153.2, 148.9, 142.2, 130.1, 128.7, 122.6, 119.1, 115.9, 110.1, 109.9, 61.5, 56.0, 55.9, 53.7, 39.8, 30.2, 25.6, 23.8; ESI-MS: 384.2 $[M + H]^+$.

*4.1.5. (E)-1-(4-hydroxy-3-methoxyphenyl)-3-(3-hydroxyphenyl)prop-2-en-1-one (**12**)*

A mixture of compound **4** (0.26 mmol), $AlCl_3$ (1.05 mmol) in CH_2Cl_2 (2.0 mL), was stirred at room temperature for 6 h under argon atmosphere. The reaction mixture then poured into ice water, stirred for 10 min, and extracted with dichloromethane (10 mL × 3). The combined organic phases were washed with saturated aqueous sodium chloride, dried over sodium sulfate, filtered and concentrated under reduced pressure to give compounds **12** as a yellow solid without further purification; 82.0% yield.

*4.1.6. General procedure for the synthesis of **13a-b***

The mixture of secondary amine (0.77 mmol) and paraformaldehyde (0.77 mmol) in ethanol was refluxed for 1 h, until paraformaldehyde was dissolved. The compound **12** (0.39 mmol) was then added in one portion. The reaction mixture was refluxed for 48 h. Ethanol was then removed under vacuum. The residue was diluted with water and extracted with dichloromethane (10 mL × 3), the combined organic phases were washed with saturated aqueous sodium chloride, dried over sodium sulfate, filtered and concentrated under reduced pressure. The residue was purified on a silica gel chromatography using mixtures of petroleum ether/ethyl acetate (3:1) as eluent to give the corresponding compounds **13a-b**.

*4.1.6.1. (E)-3-(4-((diethylamino)methyl)-3-hydroxyphenyl)-1-(3-((diethylamino)methyl)-4-hydroxy- 5-methoxyphenyl)prop-2-en-1-one (**13a**)*. It was obtained from **12** and diethylamine according to the general procedure and gave compound **13a** as a yellow oil; 51.0% yield; ^{1}H NMR (600 MHz, $CDCl_3$) δ 7.69 (d, J = 15.6 Hz, 1H), 7.51 (s, 1H), 7.49 (d, J = 15.6 Hz, 1H), 7.38 (s, 1H), 7.11 (s, 1H), 7.01–6.97 (m, 2H), 3.94 (s, 3H), 3.79 (s, 2H), 3.74 (s, 2H), 2.68–2.59 (m, 8H), 1.14–1.08 (m, 12H); ESI-MS: 441.3 $[M + H]^+$.

*4.1.6.2. (E)-1-(4-hydroxy-3-methoxy-5-(piperidin-1-ylmethyl)phenyl)-3-(3-hydroxy-4-(piperidin-1-yl methyl)phenyl)prop-2-en-1-one (**13b**)*. It was obtained from **12** and piperidine according to the general procedure and gave compound **13b** as a yellow soild; mp 76.3–78.5 °C; ^{1}H NMR (600 MHz, $CDCl_3$) δ 7.72 (d, J = 15.6 Hz, 1H), 7.54 (s, 1H), 7.51 (d, J = 15.6 Hz, 1H), 7.40 (s, 1H), 7.15 (s, 1H), 7.04–6.99 (m, 2H), 3.96 (s, 3H), 3.79 (s, 2H), 3.71 (s, 2H), 2.64 (brs, 8H), 1.69–1.66 (m, 8H), 1.51 (brs, 4H); ESI-MS: 465.3 $[M + H]^+$.

*4.1.7. General procedure for the synthesis of **19–21***

To a mixture of the corresponding benzoic acid (**16–18**) (2.35 mmol), EDCI (3.53 mmol), HOBt (3.53 mmol) and triethylamine (4.70 mmol) in dry THF was added 3-(aminomethyl)phenol. The reaction mixture was stirred for 24 h at room temperature. Solvent was removed under reduced pressure. The residue was diluted in water and extracted with dichloromethane (15 mL × 3). The combined organic phases were washed with saturated aqueous sodium chloride, dried over sodium sulfate, filtered and concentrated under reduced pressure. The residue was purified on a silica gel chromatography using mixtures of dichloromethane/ethyl acetate (30:1) as eluent to give the corresponding intermediates **19–21**.

*4.1.7.1. N-(3-hydroxybenzyl)-4-methoxybenzamide (**19**)*. It was obtained from 4-methoxybenzoic acid (**16**) and 3-(aminomethyl) phenol according to the general procedure and gave compound **19** as an oil; 48.5% yield; ^{1}H NMR (600 MHz, $CDCl_3$) δ 7.69 (d, J = 8.4 Hz, 2H), 7.35 (s, 1H), 7.15 (t, J = 7.8 Hz, 1H), 6.85–6.77 (m, 4H), 6.52 (brs, 1H), 4.52 (d, J = 5.4 Hz, 2H), 3.80 (s, 3H).

*4.1.7.2. N-(3-hydroxybenzyl)-3,4-dimethoxybenzamide (**20**)*. It was obtained from 3,4-dimethoxybenzoic acid (**17**) and 3-(aminomethyl) phenol according to the general procedure and gave compound **20** as a white solid; 60.0% yield; mp 84.3–85.2 °C; ^{1}H NMR (600 MHz, $CDCl_3$) δ 7.39 (s, 1H), 7.25 (d, J = 8.4 Hz, 1H), 7.16 (t, J = 7.2 Hz, 1H), 6.86 (s, 1H), 6.81 (d, J = 7.2 Hz, 1H), 6.78 (d, J = 7.8 Hz, 2H), 6.58 (brs, 1H), 4.54 (d, J = 4.8 Hz, 2H), 3.89 (s, 3H), 3.84 (s, 3H).

*4.1.7.3. N-(3-hydroxybenzyl)-3,4,5-trimethoxybenzamide (**21**)*. It was obtained from 3,4,5-trimethoxybenzoic acid (**18**) and 3-(aminomethyl)phenol according to the general procedure and gave compound **21** as a white solid; 60.0% yield; mp 160.5–161.2 °C; ^{1}H NMR (400 MHz, CDCl3) δ 7.21 (t, J = 8.0 Hz, 1H), 7.00 (s, 2H), 6.87 (s, 2H), 6.78 (d, J = 8.0 Hz, 1H), 6.42 (brs, 1H), 4.57 (d, J = 5.2 Hz, 2H), 3.87 (s, 9H).

*4.1.8. General procedure for the synthesis of **22–24***

To a mixture of dimethylamine hydrochloride (1.47 mmol) and paraformaldehyde (1.47 mmol), triethylamine (1.47 mmol) in ethanol refluxed for 1 h, until paraformaldehyde was dissolved. The intermediates **19–21** (0.74 mmol) were then added in one portion. The reaction mixture was refluxed for 24–48 h. Ethanol was then removed under vacuum. The residue was diluted with water and extracted with dichloromethane (10 mL × 3). The combined organic phases were washed with saturated aqueous sodium chloride, dried over sodium sulfate, filtered and concentrated under reduced pressure. The residue was purified on a silica gel chromatography using mixtures of petroleum ether/acetone (1:1) as eluent to give the corresponding compounds **22–24**.

*4.1.8.1. N-(4-((dimethylamino)methyl)-3-hydroxybenzyl)-4-methoxybenzamide (**22**)*. It was obtained from **19** and dimethylamine hydrochloride according to the general procedure and gave compound **22** as a white solid; 50.0% yield; mp 132.7–135.2 °C; ^{1}H NMR (400 MHz, $CDCl_3$) δ 7.75 (d, J = 8.4 Hz, 2H), 6.95–6.89 (m, 3H), 6.81 (s, 1H), 6.76 (d, J = 7.2 Hz, 1H), 6.36 (brs, 1H), 4.55 (d, J = 5.6 Hz, 2H), 3.77 (s, 3H), 3.65 (s, 2H), 2.35 (s, 6H), ^{13}C NMR (150 MHz, $CDCl_3$) δ 166.9, 162.0, 158.1, 139.3, 128.8, 128.8, 126.5, 120.6, 118.3, 115.1, 113.6, 62.0, 55.3, 44.2, 43.6; ESI-MS: 315.2 $[M + H]^+$.

*4.1.8.2. N-(4-((dimethylamino)methyl)-3-hydroxybenzyl)-3,4-dimethoxybenzamide (**23**)*. It was obtained from **20** and dimethylamine hydrochloride according to the general procedure and gave compound **23** as a white solid; 47.0% yield; mp 52.5–53.8 °C; ^{1}H NMR (400 MHz, $CDCl_3$) δ 7.46 (s, 1H), 7.29 (d, J = 8.4 Hz, 1H), 6.95 (d, J = 7.6 Hz, 1H), 6.86–6.83 (m, 2H), 6.77 (d, J = 7.6 Hz, 1H), 6.39 (brs, 1H), 4.56 (d, J = 4.4 Hz, 2H), 3.91 (s, 6H), 3.65 (s, 2H), 2.34 (s, 6H). ^{13}C NMR (150 MHz, $CDCl_3$) δ 166.9, 158.2, 151.6, 148.8, 139.2, 128.7, 126.9, 120.8, 119.4, 118.3, 115.2, 110.6, 110.2, 62.1, 55.9, 44.4, 44.3, 43.8; ESI-MS: 345.2 $[M + H]^+$.

*4.1.8.3. N-(4-((dimethylamino)methyl)-3-hydroxybenzyl)-3,4,5-trimethoxybenzamide (**24**)*. It was obtained from **21** and dimethylamine hydrochloride according to the general procedure and gave compound **24** as a light yellow solid; 52.0% yield; mp 49.8–51.6 °C; ^{1}H NMR (600 MHz, $CDCl_3$) δ 7.03 (s, 2H), 6.95 (d, J = 7.8 Hz, 1H), 6.82 (s, 1H), 6.77 (d, J = 7.8 Hz, 1H), 6.42 (brs, 1H), 4.56 (d, J = 5.4 Hz, 2H), 3.89 (s, 9H), 3.65 (s, 2H), 2.34 (s, 6H); ^{13}C NMR (150 MHz, $CDCl_3$) δ 166.9, 158.1, 153.0, 140.7, 139.1, 129.7, 128.7, 120.7, 118.4, 115.2, 104.4, 62.1, 60.8, 56.2, 44.2, 43.8; ESI-MS: 375.2 $[M + H]^+$.

4.2. Biological evaluation

4.2.1. Inhibition experiments of AChE and BuChE

The *in vitro* cholinesterase activities were assessed following the modified Ellman's method [42], using purified AChE from *Electrophorus electricus* (Sigma-Aldrich Co.) and purified BuChE from rat serum. The enzymatic reactions took place in 96-well plates in solutions containing acetylthiocholine iodide (1 mmol/L, 30 μL), or butyrylthiocholine iodide (1 mmol/L, 30 μL), phosphate-buffered solution (0.1 mmol/L,

pH = 7.4, 40 μL), *Ee*AChE (0.05 U/mL) or 25% serum (10 μL) and different concentrations of test compounds (20 μL) was incubated at 37 °C for 15 min. After that, 30 μL 5, 5′-dithiobis-2-nitrobenzoic acid (DTNB) solution was added into the mixture to produce the yellow anion of 5-thio-2-nitro-benzoic acid. The rate of absorbance change was measured at 405 nm in a Varioskan Flash Multimode Reader (Thermo Scientific). The *Ee*AChE inhibition assay was carried out in a phosphate buffer (0.01 mmol/L, pH = 8.0, 40 μL) with the same procedure as above, and changes in absorbance were detected at 412 nm. All samples performed in triplicate, and donepezil was applied as the positive drug. IC_{50} values were calculated and standard error of the mean was established.

4.2.2. Kinetic characterization of AChE inhibition

Kinetic characterization of the inhibition of AChE was performed according to an established method [12]. Three different concentrations of test compound were added into the solution containing 0.1 M phosphate buffer (pH = 8.0), 30 μL of 0.2% DTNB, 10 μL of 0.5 U/mL *Ee*AChE and 20 μL of substrate (ATCh). Then, the assay solution was pre-incubated for 15 min at 37 °C with the *Ee*AChE followed by the addition of substrate in different concentrations. Kinetic characterization of the hydrolysis of ATCh catalyzed by AChE was executed spectrometrically at 412 nm. The parallel control was performed each time with no inhibitor. The plots were assessed by a weighted least squares analysis. Slopes of reciprocal plots were then plotted against the concentration of **7c** for AChE to determine the reversible inhibition constant (K_i).

4.2.3. Molecular docking of AChE

The crystal structure of AChE complexed with donepezil (PBD code: *1EVE*) was obtained from the Protein Data Bank with non-bonded inhibitors and water molecules. The 3D Structure of **7c** was built and performed geometry optimization by molecular mechanics. The further preparation of the inhibitor was accomplished, which involved removing of hydrogen atoms, addition of Gasteiger charges and their atomic charges to skeleton atoms, and finally, the assignment of proper atomic types. The rotatable bonds were detected automatically by AUTODOCK 4.2 program. Polar hydrogen atoms were added to amino acid residues and Gasteiger charges were assigned to all atoms of the enzyme, with the use of Autodock Tools (ADT; version 1.5.6). The resulting enzyme structure was used as an input for the AUTOGRID program. AUTOGRID performed a pre-calculated atomic affinity grid maps for each atom type in the ligand, plus an electrostatics map and a separate desolvation map presented in the substrate molecule. All maps were calculated with 0.375 Å spacing between grid points. The center of the grid box was placed at the center of donepezil with coordinates × = 2.023, y = 63.295, z = 67.062. The dimensions of the active site box were set at 60 × 60 × 60 Å. Flexible ligand docking was performed for the compounds and each docked system was performed by 100 runs of the AUTODOCK search by the Lamarckian genetic algorithm (LGA). A cluster analysis was performed on the docking results using a root mean square (RMS) tolerance of 1.0 and the lowest energy conformation of the highest populated cluster was selected for analysis. Graphic manipulations and visualizations were done by Autodock Tools or Discovery Studio 2.5 software.

4.2.4. Antioxidant activity assay

The antioxidant activity was evaluated by oxygen radical absorbance capacity-fluorescein assay (ORAC-FL) [43]. All the assays were conducted in the wells of a black 96-well plate, containing 75 mM phosphate buffer (pH = 7.4), antioxidant (20 μL) and Fluorescein (120 μL, 150 nM final concentration). The mixture was pre-incubated for 15 min at 37 °C, and then 2,2′-Azo-bis(amidinopropane)dihydrochloride (AAPH) solution (60 μL, 12 mM final concentration) was added rapidly. The plate was placed in a Varioskan Flash Multimode Reader (Thermo Scientific) immediately, and the fluorescence recorded every minute for 90 min with excitation at 485 nm and emission at 535 nm. The plate was automatically shaken prior to each reading. Trolox (6-Hydroxy-2,5,7,8-tetramethylchromane-2-carboxylic acid), a vitamin E analogue, was used as standard (1–8 μM, final concentration). A blank (FL + AAPH) using phosphate buffer instead of antioxidant and Trolox calibration were carried out in each assay. The samples were performed at different concentration (1–10 μM). All the reaction mixture was prepared in duplicate, and at least three independent assays were performed for each sample. Antioxidant curves (fluorescence versus time) were normalized to the curve of the blank in the same assay, and then the area under the fluorescence decay curve (AUC) was calculated. The net AUC of a sample was obtained by subtracting the AUC of the blank. ORAC-FL values were expressed as Trolox equivalents by using the standard curve calculated for each sample, where the ORAC-FL value of Trolox was taken as 1, indicating the antioxidant potency of the tested compounds.

4.2.5. Metal-chelating studies

The metal chelating studies were performed in a Shimadzu UV-2450 spectrophotometer [4,45]. The UV absorption spectra of compound **7c** alone or in the presence of $CuCl_2$, $ZnCl_2$, $AlCl_3$, and $FeSO_4$ were recorded with wavelength ranging from 200 to 500 nm after incubating for 30 min at room temperature. The final volume of reaction mixture was 1 mL, and the final concentrations of tested compound and metals were 37.5 μM. The difference UV–vis spectra due to complex formation was obtained by numerical subtraction of the spectra of the metal alone and the compound alone (at the same concentration used in the mixture) from the spectra of the mixture.

To determine the stoichiometry of the complex compound-metal, the molar ratio method was used by titrating the methanol solution of tested compound with growing amounts of $CuCl_2$. The final concentration of tested compound was 37.5 μM, and the final concentration of Cu^{2+} ranged from 3.75 to 150 μM. The UV spectra were recorded and treated by numerical subtraction of $CuCl_2$ and **7c** at corresponding concentrations, plotted versus the mole fraction of **7c**.

4.2.6. Inhibition of self- and Cu^{2+}-induced $A\beta_{1-42}$ aggregation

The inhibition of self-induced $A\beta_{1-42}$ aggregation was evaluated using a Thioflavin T (ThT) -binding assay [44,45]. Test compounds were prepared in DMSO at a concentration of 2.5 mM and diluted with phosphate buffer solution (pH = 7.4) before use. HFIP pretreated $A\beta_{1-42}$ samples (Sigma Co.) was resolubilized in dry DMSO to a final stock concentration of 200 μM and was kept frozen at −80 °C until use. $A\beta_{1-42}$ (20 μL, 25 μM, final concentration) was incubated with 20 μL of test compounds at different concentrations ranging from 10 to 50 μM in 50 mM phosphate buffer solution (pH = 7.4) at 37 °C for 24 h. Wells were covered to minimize evaporation and incubated without exposure to light at room temperature. After the incubation, 160 μL of 5.0 μM thioflavin T in 50 mM glycine-NaOH buffer (pH = 8.5) was added to each well. Each measurement was run in triplicate and each reaction was repeated for at least three times. Fluorescence was performed on a Varioskan Flash Multimode Reader (Thermo Scientific) with excitation and emission wavelengths at 446 nm and 490 nm, respectively. The fluorescence intensities were recorded, and the percentage of inhibition on aggregation was calculated by using the following formula: $(1\text{-}IF_i/IF_c) \times 100$, in which IF_i and IF_c were the fluorescence intensities obtained for $A\beta_{1-42}$ in the presence and in the absence of inhibitors, respectively.

For the inhibition of Cu^{2+}-induced $A\beta_{1-42}$ aggregation assay, the $A\beta_{1-42}$ stock solution was diluted in HEPES buffer (20 mM, pH = 6.6, 150 mM NaCl), and solutions of Cu^{2+} were prepared from standards to concentration of 75 μM using the HEPES buffer (20 mM, pH = 6.6, 150 mM NaCl). 190 μL of 5 μM thioflavin T in 50 mM glycine-NaOH buffer (pH = 8.5) was added to a mixture of the peptide (20 μL, 25 μM, final concentration) and Cu^{2+} (20 μL, 25 μM, final concentration), with or without the tested compound at different concentrations (20 μL, 10–35 μM, final concentration) after incubated at 37 °C for 24 h. The

detection method was the same as above.

4.2.7. In vitro inhibition of MAO activity

To further study the biological profile of target compounds, the inhibitory activity against MAO-A and MAO-B was determined [46]. Recombinant human MAO-A and -B were obtained from commercial sources (Sigma Co.), pre-aliquoted and stored at −80 °C. Solutions of the target compounds were prepared in DMSO in 2.5 mM for storage and diluted with potassium phosphate buffer (100 mM, pH = 7.40, containing KCl 20.2 mM) before use. The enzymatic reactions were conducted in potassium phosphate buffer (pH = 7.4, made isotonic with KCl) to a final volume of 500 µL containing kynuramine, various concentrations of the test compounds and 4% DMSO as cosolvent. The addition of MAO-A or -B (7.5 µg/mL) is a trigger of the reaction, after then the mixture was incubated for 30 min at 37 °C. The reactions were ended by the addition of 400 µL NaOH (2.0 mol/L) and 1000 µL water and then centrifuged at 16,000 g for 10 min .The rates of MAO catalysis can be conveniently determined by measuring the formation of 4-hydroxyquinoline via fluorescence spectrophotometry at excitation and emission wavelengths of 310 nm and 400 nm, respectively. Samples containing 4-hydroxyquinoline (0.047–1.56 µM) dissolved in 500 µL potassium phosphate buffer were prepared to give a linear calibration curve. IC_{50} values were estimated from sigmoidal dose-response curves (graphs of the initial rate of kynuramine oxidation versus the logarithm of inhibitor concentration) and were determined in triplicate and are expressed as mean ± standard deviation (SD). Each measurement was run in triplicate and each reaction was repeated for at least three times.

4.2.8. Molecular modeling study of MAO

Docking studies were performed using AUTODOCK 4.2 program. Each docking system was performed by 100 runs of the Autodock using the Lamarckian genetic algorithm (LGA). The X-ray crystal structures of hMAO-A (PDB: *2Z5X*) and hMAO-B (PDB: *2 V60*) were obtained from the Protein Data Bank [47]. The original ligands and water molecules were removed and hydrogen atoms were added onto both proteins and cofactors. The lowest docking-energy conformation of the highest populated cluster was considered as the most stable orientation and could be selected for analysis. A cluster analysis was performed on the docking results using a root mean square (RMS) tolerance of 1.0. Graphic manipulations and visualizations were done by Autodock Tools or Discovery Studio 2.5 software.

4.2.9. In vitro blood–brain barrier permeation assay

To evaluate the *in vitro* BBB permeation assay of the compounds, the method described by Di *et al.* was conducted [48]. The donor plate (MATRNPS50) and the acceptor plate (PVDF membrane, pore size is 0.45 µm, MAIPN4550) were both purchased from Millipore. Filter PDVF membrane units (diameter 25 mm, pore size 0.45 µm) from Pall Corporation were used to filter the samples. Commercial drugs were purchased from Sigma and Alfa Aesar. Porcine brain lipid (PBL) was obtained from Avanti Polar Lipids. Test compounds (100 µg/mL, final concentration) were dissolved in DMSO at 5 mg/mL and diluted 50-fold in PBS/EtOH (70:30). Then 350 µL of the diluted compound solution (100 µg/mL) was added to the donor wells. The acceptor wells were filled with 200 µL of PBS/EtOH (70:30). The filter membrane was coated with PBL in dodecane (selected empirically as 4 µL volume of 20 µg/mL PBL in dodecane). The acceptor filter plate was carefully put on the donor plate to form a sandwich (consisting of the aqueous donor with test compound on the bottom, lipid membrane in the middle and the aqueous acceptor on the top), which was left undisturbed for 18 h at 25 °C. After incubation, the donor plate was removed and the concentration of the compounds in the acceptor and donor wells was determined using the Varioskan Flash Multimode Reader (Thermo Scientific). Permeability rates (Pe) was calculated using the following expression: $P_e = -\ln [1 - C_A(t)/C_{equilibrium}]/[A \times (1/V_D + 1/V_A) \times t]$ $C_{equilibrium} = [C_D(t) \times V_D + C_A(t) \times V_A]/(V_D + V_A)$, where A is the filter area, t is the permeation time, V_D is the volume of donor well, V_A is the volume in the acceptor well, $C_A(t)$ is the compound concentration in acceptor well at time t, and $C_D(t)$ is the compound concentration in donor well at time t. Eleven quality control standards of known BBB permeability were used to monitor the consistency of each experiment. Every sample was analyzed at ten wavelengths in four wells and in at least three independent runs. The results were given as the mean ± standard deviation.

Acknowledgments

This work was supported by Sichuan Science and Technology Program (2018SZ0014) and the National Science and Technology Major Project on “Key New Drug Creation and Manufacturing Program” (2013ZX09301304-002).

Appendix A. Supplementary material

Supplementary data to this article can be found online at https://doi.org/10.1016/j.bioorg.2019.03.043.

References

[1] A.M. Palmer, Neuroprotective therapeutics for Alzheimer's disease: progress and prospects, Trends Pharm. Sci. 32 (2011) 141–147.
[2] S.Y. Hung, W.M. Fu, Drug candidates in clinical trials for Alzheimer's disease, J. Biomed. Sci. 24 (2017) 47.
[3] N. Jiang, S.Y. Li, S.S. Xie, Z.R. Li, K.D. Wang, X.B. Wang, L.Y. Kong, Design, synthesis and evaluation of multifunctional salphen derivatives for the treatment of Alzheimer's disease, Eur. J. Med. Chem. 87 (2014) 540–551.
[4] Q. Song, Y. Li, Z.C. Cao, H.Y. Liu, C.Q. Tiana, Z.Y. Yang, X.M. Qiang, Z.H. Tan, Y. Deng, Discovery of novel 2,5-dihydroxyterephthalamide derivatives as multi-functional agents for the treatment of Alzheimer's disease, Bioorg. Med. Chem. 26 (2018) 6115–6127.
[5] X.Q. Wang, C.L. Xia, S.B. Chen, J.H. Tan, T.M. Ou, S.L. Huang, D. Li, L.Q. Gu, Z.S. Huang, Design, synthesis, and biological evaluation of 2-arylethenylquinoline derivatives as multifunctional agents for the treatment of Alzheimer's disease, Eur. J. Med. Chem. 89 (2015) 349–361.
[6] V. Capurro, P. Busquet, J.P. Lopes, R. Bertorelli, G. Tarozzo, M.L. Bolognesi, D. Piomelli, Pharmacological characterization of memoquin, a multi-target compound for the treatment of Alzheimer's disease, Plos. One. 8 (2013) 56870.
[7] Q. Liu, X.M. Qiang, Y. Li, Z.P. Sang, Y.X. Li, Z.H. Tan, Y. Deng, Design, synthesis and evaluation of chromone-2-carboxamido-alkylbenzylamines as multifunctional agents for the treatment of Alzheimer's disease, Bioorg. Med. Chem. 23 (2015) 911–923.
[8] Y. Li, X.M. Qiang, L. Luo, et al., Multitarget drug design strategy against Alzheimer's disease: Homoisoflavonoid Mannich base derivatives serve as acetylcholinesterase and monoamine oxidase B dual inhibitors with multifunctional properties, Bioorg. Med. Chem. 25 (2017) 714–726.
[9] I. Bolea, A. Gella, M. Unzeta, Propargylamine-derived multitarget-directed ligands: fighting Alzheimer's disease with monoamine oxidase inhibitors, J. Neural Transm. 120 (2013) 893–902.
[10] L. Luo, Y. Li, X.M. Qiang, et al., Multifunctional thioxanthone derivatives with acetylcholinesterase, monoamine oxidases and β-amyloid aggregation inhibitory activities as potential agents against Alzheimer's disease, Bioorg. Med. Chem. 25 (2017) 1997–2009.
[11] H.L. Zheng, M. Fridkin, M. Youdim, From single target to multi-target/network therapeutics in Alzheimer's therapy, Pharm. 7 (2014) 113–135.
[12] C.J. Lu, Q. Zhou, J. Yan, Z.Y. Du, L. Huang, X.S. Li, A novel series of tacrine-selegiline hybrids with cholinesterase and monoamine oxidase inhibition activities for the treatment of Alzheimer's disease, Eur. J. Med. Chem. 62 (2013) 745–753.
[13] J.S. Choi, M.N. Islam, M.Y. Ali, Y.M. Kim, H.J. Park, H.S. Sohn, H.A. Jung, The effects of C-glycosylation of luteolin on its antioxidant, anti-Alzheimer's disease, anti-diabetic, and anti-inflammatory activities, Archiv. Pharm. Res. 37 (2014) 1354–1363.
[14] D. Pratico, Evidence of oxidative stress in Alzheimer's disease brain and antioxidant therapy: lights and shadows, Ann. N. Y. Acad. Sci. 1147 (2008) 70–78.
[15] A.I. Bush, M.O. Chohan, Drug development based on the metals hypothesis of Alzheimer's disease, J. Alzheimer's Dis. 15 (2008) 223–240.
[16] T. Mohamed, A. Shakeri, P.P.N. Rao, Amyloid cascade in Alzheimer's disease: recent advances in medicinal chemistry, Eur. J. Med. Chem. 113 (2016) 258–272.
[17] A. Agis-Torres, M. Sölhuber, M. Fernandez, J.M. Sanchez-Montero, Multi-target-directed ligands and other therapeutic strategies in the search of a real solution for Alzheimer's disease, Curr. Neuro. 12 (2014) 2–36.
[18] C. Zhang, Q.Y. Du, L.D. Chen, et al., Design, synthesis and evaluation of novel tacrine-multialkoxybenzene hybrids as multi-targeted compounds against Alzheimer's disease, Eur. J. Med. Chem. 116 (2016) 200–209.
[19] F. Prati, A. Cavalli, M.L. Bolognesi, Navigating the chemical space of multitarget-directed ligands: from hybrids to fragments in Alzheimer's disease, Molecules 21

(2016) 466–478.
[20] M. Bajda, N. Guzior, M. Ignasik, B. Malawska, Multi-target-directed ligands in Alzheimer's disease treatment, Curr. Med. Chem. 18 (2011) 4949–4975.
[21] X. Chen, M. Decker, Multi-target compounds acting in the central nervous system designed from natural products, Curr. Med. Chem. 20 (2013) 1673–1685.
[22] R. León, A.G. Garcia, J. Marco-Contelles, Recent advances in the multi-target directed ligands approach for the treatment of Alzheimer's disease, Med. Res. Rev 33 (2013) 139–189.
[23] F. Prati, E. Uliassi, M.L. Bolognesi, Two diseases, one approach: multi-target drug discovery in Alzheimer's and neglected tropical diseases, Med. Chem. Comm 5 (2014) 853.
[24] S.S. Xie, J.S. Lan, X.B. Wang, N. Jiang, G. Dong, Z.R. Li, K.D. Wang, P.P. Guo, L.Y. Kong, Multifunctional tacrine-trolox hybrids for the treatment of Alzheimer's disease with cholinergic, antioxidant, neuroprotective and hepatoprotective properties, Eur. J. Med. Chem. 93 (2015) 42–50.
[25] Z.C. Cao, J. Yang, R. Xu, et al., Design, synthesis and evaluation of 4'-OH-flurbiprofen-chalcone hybrids as potential multifunctional agents for Alzheimer's disease treatment, Bioorg. Med. Chem. 26 (2018) 1102–1115.
[26] G.Y. Xiao, Y. Li, X.M. Qiang, et al., Design, synthesis and biological evaluation of 4'-aminochalcone-rivastigmine hybrids as multifunctional agents for the treatment of Alzheimer's disease, Bioorg. Med. Chem. 25 (2017) 1030–1041.
[27] J.W. Choi, B.K. Jang, N.C. Cho, et al., Synthesis of a series of unsaturated ketone derivatives as selective and reversible monoamine oxidase inhibitors, Bioorg. Med. Chem. 23 (2015) 6486–6496.
[28] T. Fuchigami, Y. Yamashita, M. Haratake, et al., Synthesis and evaluation of ethyleneoxylated and allyloxylated chalcone derivatives for imaging of amyloid β plaques by SPECT, Bioorg. Med. Chem. 22 (2014) 2622 2622-2268.
[29] S. Bag, S. Ghosh, R. Tulsan, et al., Design, synthesis and biological activity of multifunctional α, β-unsaturated carbonyl scaffolds for Alzheimer's disease, Bioorg. Med. Chem. Lett. 23 (2013) 2614–2618.
[30] D.H. Park, J. Venkatesan, S.K. Kim, V. Ramkumar, P. Parthiban, Antioxidant properties of Mannich bases, Bioorg. Med. Chem. Lett. 22 (2012) 6362–6367.
[31] G. Roman, Mannich bases in medicinal chemistry and drug design, Eur. J. Med. Chem. 89 (2015) 743–816.
[32] N. Buyukkidan, S. Ozer, Synthesis and characterization of Ni (II) and Cu (II) complexes derived from novel phenolic Mannich bases, Turk. J. Chem. 37 (2013) 101–110.
[33] T.H. Bui, T.T. Le, T.T. Vu, X.T. Hoang, synthesis and *in vitro* cytotoxic activity evaluation of new Mannich bases, B. Kor. Chem. Soc. 33 (2012) 1586–1592.
[34] S.K. Shahabuddin, R. Munikishore, G. Trimurtulu, et al., Two new chalcones from the flowers of Clerodendrum inerme, Nat. Prod. Commun. 8 (2013) 459–460.
[35] S. Iwata, T. Nishino, N. Nagata, et al., Antitumorigenic activities of chalcones. I. Inhibitory effects of chalcone derivatives on 32Pi-incorporation into phospholipids of HeLa cells promoted by 12-O-tetradecanoyl-phorbol 13-acetate (TPA), Biol. Pharm. Bull. 18 (1995) 1710.
[36] A. Wilhelm, P. Kendrekar, A. Noreljaleel, et al., Syntheses and *in vitro* antiplasmodial activity of aminoalkylated chalcones and analogues, J. Nat. Prod. 78 (2015) 1848–1858.
[37] A. Wacek, Model experiments on lignin cleavage. II. Action of alkali and sodium ethylate on substituted chalcones and dehydrodiisoeugenol methyl ether, Ber. Dtsch. Chem. Ges. 70 (1937) 190–195.
[38] A. Wilhelm, P. Kendrekar, A.E. Noreljaleel, E.T. Abay, S.L. Bonnet, L. Wiesner, C. de Kock, Syntheses and *in vitro* antiplasmodial activity of aminoalkylated chalcones and analogues, J. Nat. Prod. 78 (2015) 1848–1858.
[39] A.S. Negi, S.K. Chattopadhyay, S. Srivastava, A.K. Bhattacharya, A simple regioselective demethylation of *p*-aryl methyl ethers using aluminum chloride-dichloromethane system, Syn. Comm. 35 (2005) 15–21.
[40] Z.Z. Wei, Y.T. Gong, T.Y. Xiong, P.F. Zhang, H.R. Li, Y. Wang, Highly efficient and chemoselective hydrogenation of α, β-unsaturated carbonyls over Pd/N-doped hierarchically porous carbon, Catal. Sci. Technol. 5 (2015) 397–404.
[41] R. Chinchilla, D.J. Dodsworth, C. Nájera, J.M. Soriano, Ammonium salts from polymer-bound *N*-hydroxysuccinimide as solid-supported reagents for EDC-mediated amidations, Tetra. Lett. 44 (2003) 463–466.
[42] Y. Li, X.M. Qiang, L. Luo, X. Yang, G.Y. Xiao, Q. Liu, J.C. Ai, Z.H. Tan, Y. Deng, Aurone Mannich base derivatives as promising multifunctional agents with acetylcholinesterase inhibition, anti-b-amyloid aggragation and neuroprotective properties for the treatment of Alzheimer's disease, Eur. J. Med. Chem. 126 (2017) 762–775.
[43] L. Huang, C.J. Lu, Y. Sun, F. Mao, Z.H. Luo, T. Su, H.L. Jiang, W.J. Shan, X.S. Li, Multitarget-directed benzylideneindanone derivatives: anti-beta-amyloid (Aβ) aggregation, antioxidant, metal chelation, and monoamine oxidase B (MAO-B) inhibition properties against Alzheimer's disease, J. Med. Chem. 55 (2012) 8483–8492.
[44] M. Rosini, E. Simoni, M. Bartolini, A. Cavalli, L. Ceccarini, N. Pascu, D.W. Mcclymont, Inhibition of acetylcholinesterase, β-amyloid aggregation, and NMDA receptors in Alzheimer's disease: a promising direction for the multi-target-directed ligands gold rush, J. Med. Chem. 51 (2008) 4381–4384.
[45] P. Camps, X. Formosa, C. Galdeano, D. Munoz-Torrero, L. Ramirez, E. Gomez, N. Isambert, Pyrano[3,2-c]quinoline-6-chlorotacrine hybrids as a novel family of acetylcholinesterase- and β-amyloid-directed anti-Alzheimer compounds, J. Med. Chem. 52 (2009) 5365–5379.
[46] L.J. Legoabe, A. Petzer, J.P. Petzer, Selected C_7-substituted chromone derivatives as monoamine oxidase inhibitors, Bioorg. Chem. 45 (2012) 1–11.
[47] N. Desideri, A. Bolasco, R. Fioravanti, et al., Homoisoflavonoids: natural scaffolds with potent and selective monoamine oxidase-B inhibition properties, J. Med. Chem. 54 (2011) 2155–2164.
[48] L. Di, E.H. Kerns, K. Fan, O.J. McConnell, G.T. Carter, High throughput artificial membrane permeability assay for blood–brain barrier, Eur. J. Med. Chem. 38 (2003) 223–232.